Spectral Analysis of Channel-Flow DNS Data at $Re_\tau = 4200$ with Emphasis on the Attached-Eddy Hypothesis

Lionel Agostini[1, 2, a)] and Michael Leschziner[2, b)]

[1)] *Mechanical and Aerospace Engineering*

The Ohio State University

Columbus,Ohio 43210, USA

[2)] *Department of Aeronautics*

Imperial College London

South Kensington, London, SW7 2AZ, UK

DNS data for channel flow at a friction Reynolds number of 4200, generated by Lozano-Durán & Jiménez (JFM, vol 759, 2014), are used to examine the properties of near-wall turbulence within sub-ranges of eddy-length scale. Attention is primarily focused on the intermediate layer ("meso-layer") covering the logarithmic velocity region within the range of wall-scaled wall-normal distance of 80-1500. The examination is based on a number of statistical properties, including pre-multiplied and compensated spectra, pre-multiplied derivative of the second-order structure function and three scalar parameters that characterise the anisotropic or isotropic state of the various length-scale sub-ranges. This analysis leads to the delineation of three regions within the map of wall-normal-wise pre-multiplied spectra, each characterized by distinct turbulence properties. A question of particular interest is whether the Townsend-Perry Attached Eddy Hypothesis (AEH) can be shown to be valid across the entire meso-layer, in contrast to the usual focus on the outer portion of the logarithmic-velocity layer at high Reynolds numbers, which is populated with very large-scale motions. This question is addressed by reference to properties in the pre-multiplied scale-wise derivative of the second-order structure function (PMDS2) and joint PDFs of streamwise-velocity fluctuations and their streamwise and spanwise derivatives. This examination provides evidence, based primarily on the existence of a plateau region in the PMDS2 for the qualified validity of the AEH right down the lower limit of the logarithmic velocity range.

Keywords: near-wall turbulence, channel flow, eddy scales, scale-wise anisotropy, spectra, structure function

[a)]l.agostini@imperial.ac.uk

[b)]mike.leschziner@imperial.ac.uk

I. INTRODUCTION

The Townsend-Perry Attached-Eddy Hypothesis (AEH; Townsend[1] and Perry et al.[2,3]) is one of the major historical fix-points of sheared near-wall turbulence. Its most important statistical constituent is the statement that the energy-containing motions in the log-layer are associated with coherent eddies that are "attached" to the wall, both, their dimension and their energy, rising linearly with wall distance, implying that the eddies are self-similar. Perry et al.[3] thus proposed a conceptual model of a hierarchy of wall-attached eddies which increase in size by consecutive doubling and span the entire boundary layer, from the viscous scale $\delta_\nu = \nu/u_\tau$ to the outer edge δ.

The AEH is compatible with two principal statistical characteristics. One, derived by Townsend[1], is that the streamwise and spanwise turbulence-energy components $\overline{u'u'}$, $\overline{w'w'}$, respectively, decay logarithmically towards the edge of the velocity log layer. Another is that the energy spectra, within the logarithmic range of the energy components, follow the law $E_{uu}(k_x) \propto k_x^{-1}$, $E_{ww}(k_x) \propto k_x^{-1}$ – i.e., that the pre-multiplied spectra assume a constant value (Perry at al.[3,4], Nickels at al.[5]). Integration of these spectra with respect to k_x (or its inverse – the wave length) then readily yields the logarithmic variation of the related turbulence-energy components.

As the presence of k_x^{-1} variation is not easily identifiable, at least in one-dimensional spectra at moderate Reynolds-number values, Davidson et al[6,7] proposed that the second-order structure function $S_{2,u}(\delta_x) = \langle [u(x+\delta_x) - u(x)]^2 \rangle$ should provide a more sensitive indicator of the validity of the AEH. Davidson et al show that the behaviour is consistent with a logarithmic rise of $S_{2,u}(\delta_x)$ up to the integral length scale, beyond which the structure function tends to a constant value. When the structure function is scaled with the squared of the shear velocity u_τ^2, and δ_x is scaled with y, the expectation is that it should display a universal behaviour, independent of the wall distance y, and this is indeed demonstrated by Davidson et al[6,7] for two particular boundary layers at momentum-thickness Reynolds-number values $Re_\theta = 12600$ and 37500, the latter corresponding to $Re_\tau \approx 14000$. A focus on $S_{2,u}(\delta_x)$, as a diagnostic indicator of wall-normal eddy organisation and the AEH, was most recently advocated by de Silva et al[8] and Chung et al[9], the former analysing the structure of boundary layers at Re_τ up to approximately 10^6, and the latter aimed primarily at reconciling significant differences between high-Reynolds-number boundary-layer and pipe-

flow data in respect of the k_x^{-1} region in the associated spectra. In common with most studies examining aspects of the AEH, de Silva et al[8] concentrate their attention on the outer portion of the respective boundary layers, beyond the position of the plateau (or second maximum) in the wall-normal variation of the streamwise turbulence-energy component, where the second-order structure function varies logarithmically with the two-point separation and where the variations collapse if this separation is normalized by the wall distance. Based on theoretical considerations by Woodcock and Marusic[10], who provide formal support and analytical model for the AEH, de Silva et al[8] also extend their investigation to higher-order structure functions and demonstrate a logarithmic-scaling behaviour for these functions at sufficiently high Reynolds-number values and a separation distance larger than the wall distance.

Townsend's and Perry's original interpretation was that the AEH applies to the entire velocity log-law region. Studies consistent with this view are those of Davidson[6,7] and Hwang[11]. The former discusses the logarithmic behaviour of the structure function within the range $100 < y^+ < 200$, in relation to the k_x^{-1} behaviour that is observed by Nickels et al[5] to apply in the boundary layer at $Re_\theta = 37500$ over a similar y^+ range. Analyzing the implications of a sequence of minimal-channel simulations, each used to isolate the characteristics of a narrow size ranges of eddies, Hwang[11] argues that the entire log-law layer is populated, as suggested by Jiménez & Hoyas[12] and Marusic et al[13], by a hierarchical set of self-similar and self-sustaining attached eddies, in line with the original AEH. However, the above interpretation appears at odds with results derived from experimental data for high-Reynolds-number pipe flow (Hultmark et al,[14], Rosenberg et al[15]) and also DNS data for channel flow at $Re_\tau = 4200$ (Lozano-Durán & Jiménez[16,17]), which show that the logarithmic variation of $\overline{u'u'}^+$ does not apply across the intermediate portion of the velocity log-law layer – referred to as the "meso-layer" henceforth – which separates the layer below $y^+ \approx 100$ from the outer region lying beyond $y \approx 0.5\delta$ (around $y^+ = 2000$ in the channel flow considered herein). The reason is that the streamwise fluctuation-energy profile is increasingly affected, as the Reynolds number exceeds $Re_\tau \approx 1000$, by contributions arising from energetic outer structures having streamwise and spanwise length scales of order $5 - 10\delta$ and $0.5 - 1\delta$, respectively (Kim et al.[18], Del Álamo & Jiménez[19], Hutchins et al.[20]). The wall-normal variation of the streamwise energy associated with these structures is fairly flat (Marusic et al[21]), increases with Re_τ, and its (weak) maximum is reported by Marusic et al[22] to follow the

location $y^+ \approx 3.9\sqrt{Re_\tau}$ (corresponding to around 0.05δ). Importantly, the energy remains elevated well beyond this location, as well across the entire near-wall region including meso-layer and, indeed, the viscosity-affected sublayer, causing substantial friction footprints on the wall; in other words, the energy profile no longer scales with u_τ and the logarithmic variation of $\overline{u'u'}^+$ in the velocity log-law region is lost or becomes highly indistinct, at least at $Re_\tau < 5000$. As observed by Vassilicos et al.[23] , this behaviour is incompatible with the AEH, and this led them to propose a new spectral range of the form $E_{uu} = Cu_\tau^2 \delta (k_x \delta)^{-m}$ for the intermediate range, allowing them to 'predict' the rise in $\overline{u'u'}^+$ due to the outer scales.

Measurements at $Re_\tau > 7000$ by Hutchins at al[24], Hultmark et al[14,25,26] and Rosenberg et al[15] display a tendency for $\overline{u'u'}^+$ to re-establish a logarithmic-decay variation well beyond the meso-layer of the velocity log-law and also well beyond the position of maximum large-scale energy - although with a slope different from that applicable within the velocity log-law layer at much lower Reynolds-number values. This has led to a proposition that the AEH should only apply in the extreme outer layer of the velocity log-law region, on the grounds that *"determining the extend of the logarithmic layer from U^+ alone is difficult because of the slow departure from any log law"* (Smits et al[27]).

The evident controversy on the subject of the AEH - in particular, the wall-normal range to which it applies – motivated the present authors to examine the statistical properties of a channel flow at $Re_\tau = 4200$. This value is substantially lower than that achieved in experiments, but is arguably high enough to undertake a searching study by post-processing the highly resolved data that yield well-converged statistics. The DNS data were obtained with a spectral code by Lozano-Durán & Jiménez[16,17], according to well established quality criteria, over a domain $L_x = 2\pi h$, $L_z = \pi h$, with a grid containing $3072 \times 3072 \times 1081$ nodes and cell dimensions $\Delta x^+ = 12.8$, $\Delta z^+ = 6.4$, $\Delta y^+_{max} = 10.7$. Downloaded data consisted of full-volume snapshot at 40 time levels, corresponding to 15 turnovers of the global eddies. While the motivation for the present study is rooted in, and emphasis is placed on, the AEH, the analysis extends, more broadly, to an examination of the statistical properties of, and scaling laws pertaining to, different scale sub-ranges within the spectrum of turbulent fluctuations across the near-wall layer. Observations derived from this latter part turn out to be highly pertinent to the discussion on the validity of the AEH in the meso-layer.

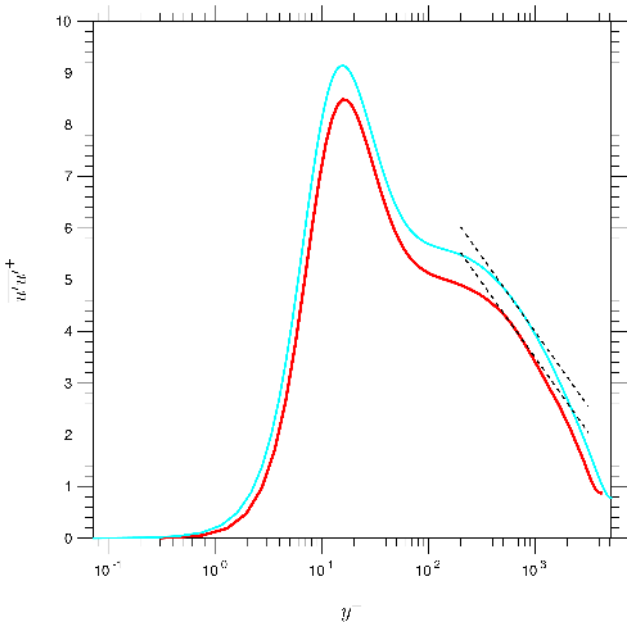

FIG. 1. Wall-normal distribution of the streamwise stress at $Re_\tau = 4200$ (red line) and $Re_\tau = 5200$ from Lee & Moser[28]. The dashed lines represents the variation $\overline{u'u'}^+ = -1.26 \log y^+ + B$, with $B = 12.2$ and 12.7 for $Re_\tau = 4200$ and $Re_\tau = 5200$, respectively.

II. STATISTICAL PROPERTIES OF EDDY-LENGTH-SCALE SUB-RANGES

Figure 1 shows profiles of the streamwise turbulence energy for $Re_\tau = 4200$ and 5200. The latter originates from a DNS study by Lee & Moser[28] for a channel flow performed over a box of $L_x = 8\pi h$, $L_z = 3\pi h$ – i.e., much larger than that exploited in the present study. Unfortunately, the raw data necessary for the analysis to follow are not available for the $Re_\tau = 5200$ case.

Attention focuses here on what is termed the "meso-layer", divided into two portions: the "plateau" region, covering $y^+ \approx 80 - 500$, and the outer layer, extending to around $y^+ \approx 2000$ - i.e., roughly $0.5h$ in the present flow. The outer portion of the meso-layer, beyond the region in which the streamwise energy features an inflection region or a (second) maximum , is populated with very large scale motions (VLSMs), and it is this layer that has been the focus of attention in studies of Vassilicos et al.[23], Hutchins at al[13], Hultmark et al[14] and Rosenberg et al[15], at $Re_\tau > 7000$, who show that the streamwise energy displays a logarithmic-decay variation at the same slope as that in figure 1. The variation of the energy in the outer layer, $500 < y^+ < 1000$, suggests a log-like decay, especially at the high

Reynolds value, and the slope of this decay is given in figure 1. Whether a logarithmic-decay law within the meso-layer is supported by other statistical properties will be examined below.

A property consistent with the log-variation of $\overline{u'u'}^+$ and with the AEH is the presence of a region of constant value in the pre-multplied spectra $k_x\Phi_{uu}$, where x is assumed statistically homogeneous. If this region is bounded by $\lambda^+_{x,min} = Cy^+$ and $\lambda^+_{x,max} = cst$, the log relationship emerges from:

$$\begin{aligned}\overline{u'u'}^+(y^+) &= \int_{\lambda^+_{x,min}}^{\lambda^+_{x,max}} k_x\phi_{uu}(y^+,\lambda^+_x)d\log(\lambda^+_x) \\ &= \int_{Cy^+}^{cst} Ad\log(\lambda^+_x) \\ &= -A\log(y^+) + B\end{aligned} \tag{1}$$

If, on the other hand, the upper limit of integration is a line parallel to that defining the lower limit – i.e. $\lambda^+_{x,max} = Dy^+$ – then $\overline{u'u'}^+(y^+) = cst$. The significance of this distinction between the two variations in the upper limits of integration will transpire in Section III.

It is important to underline that, for the AEH to be valid, the equivalent of equation 1 must also apply in respect of the spanwise spectra, i.e. $k_z\Phi_{uu}$ must also be constant within boundaries corresponding to those applicable to the streamwise spectra.

Figure 2 shows the pre-multiplied spectra for $Re_\tau = 4200$. Although there is an indication that the λ^+_x and λ^+_z locations at which the energy begins to rise steeply vary linearly with y^+, neither spectral maps features a well-defined constant-value plateau within the meso-layer, thus offering no obvious support for equation 1.

A curious feature observed in figure 2(b) is the oscillatory behaviour of the contours below and to the right of the red line, especially along the $y^+ - \lambda^+_z$ locus of maximum energy density. Although relatively mild, this behaviour is indicative of a lack of convergence of the FFT – an artefact that encourages the alternative use of the second-order structure function as a primary diagnostic means, pursued in Section III. The use of the structure function is also motivated by the fact that it is not affected by aliasing associated to the large-scale motion and thus leads to a better identification of the plateau region (see Davidson et al[6]). However, prior to this change in focus, the spectra, both those in figure 2 and others pertaining to the spanwise and wall-normal fluctuations, are used to examine some statistical properties

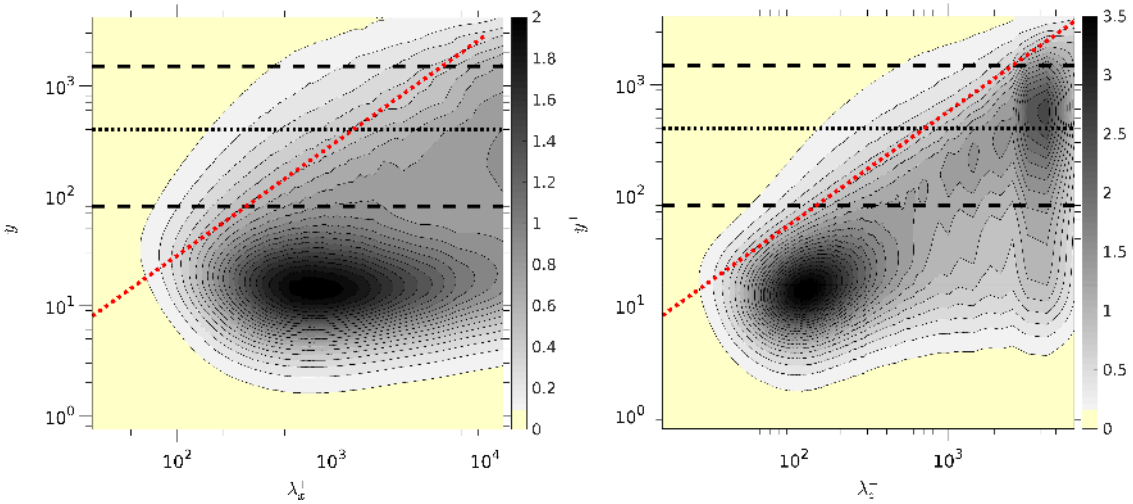

(a) (b)

FIG. 2. Pre-multiplied power spectrum of the streamwise fluctuations, in both streamwise (a) and spanwise direction (b); at $Re_\tau = 4200$. The dotted red lines show either the relation $\lambda_x^+ = 3.5y^+$ or $\lambda_z^+ = 7y^+ = 2\lambda_x^+$.

of turbulence within different spectral portions of the eddy scales. The main objective is to identify and separate sub-ranges of isotropic and anisotropic scales, the former characterizing the inertial subrange and associated with detached eddies (Jiménez[29]), and the latter – at larger scales – associated with attached eddies (Perry et al.[3], Högström et al.[30], Davidson et al[6]). This identification is pursued below.

A. Inertial Range - Detached Eddies

In order to shed light on the characteristics of scale sub-ranges, some specific manipulations of the spectral maps are proposed herein. Figure 3 shows two ways of highlighting the region in which the scales are close to being isotropic. The first entails the use of compensated spectra $\epsilon^{-2/3}k_x^{5/3}\Phi_{uu}$ and $\epsilon^{-2/3}k_z^{5/3}\Phi_{uu}$, which are shown figures 3(a) and 3(b), respectively, where ϵ is a surrogate of rate of turbulence-energy dissipation, defined such as $\epsilon = \overline{\omega_k\omega_k}/3$. The red lines in the x-wise and z-wise maps are defined, respectively, by $\lambda_x^+ = 3.5 \times y^+$ and $\lambda_z^+ = 7 \times y^+ = 2 \times \lambda_x^+$, while the blue lines describe, respectively, the variations $\lambda_x^+ = 3.5 \times (y^+)^{1/3}$ and $\lambda_z^+ = 7 \times (y^+)^{1/3} = 2 \times \lambda_x^+$. The red and blue lines bound, approximately, plateau regions characteristic of near-isotropy.

The second route rests on the definition of the following "isotropy parameter":

$$\gamma^{3c} \equiv \frac{3|\Phi_{uu}||\Phi_{vv}||\Phi_{ww}|}{|\Phi_{uu}|^3 + |\Phi_{vv}|^3 + |\Phi_{ww}|^3} \tag{2}$$

in which Φ_{uu}, Φ_{vv} and Φ_{ww} are the x-wise or z-wise spectra for the three components u, v and w, respectively. This parameter tends to a maximum of 1 in the case of isotropy, declining to zero in the case of a two-component or a one-component state. The maps in figures 3(c) and 3(d) show (for greater visual impact) the square of γ^{3c} as functions of λ_x^+ and λ_z^+, respectively. The fact that regions of high γ^{3c} are, again, bounded by the red and blue lines and broadly coincide with the near-plateau regions in the compensated spectra supports the proposition that these regions within the meso-layer characterize detached eddies.

B. Anisotopic Range – Attached Eddies and Large-Scale Motions

An analogous route to that taken in the previous sub-section to highlight isotropy by use of the parameter γ^{3c} is adopted here to identify region of elevated anisotropy. Thus, a parameter that identifies the dominance of the streamwise component over the two others is:

$$\gamma_u^{1c} \equiv \frac{|\Phi_{uu}||\Phi_{uu}|}{|\Phi_{uu}|^2 + |\Phi_{vv}|^2 + |\Phi_{ww}|^2} \tag{3}$$

This parameter tends to 1 when the energy is increasingly contained in the Φ_{uu} spectra, and diminishes when the anisotropic state departs from the one-component condition. Maps of $(\gamma_u^{1c})^3$ in the x and z directions (the cubic exponent designed to accentuate gradients in the maps) are shown in figures 4(a) and 4(b), respectively.

Both maps reveal that, within the meso-layer, the dominance of the streamwise component is confined to the larger scales beyond the boundaries identified by the red lines, and this is the attached-eddy region, as will be argued in Section III. In fact, the most pronounced regions in figure 4 pertain to scales which are the subject of many studies that deal with elongated large-scale structures in the outer part of the log-layer (Marusic[31]). Figure 4 also contains a y^+-wise profile of the normalised streamwise energy, and this provides confirmation of the existence of energetic structures in the outer layer around $y^+ = 500$. Reference to the $(\gamma_u^{1c})^3$ distribution along the dotted black line at $y^+ = 500$ clearly shows

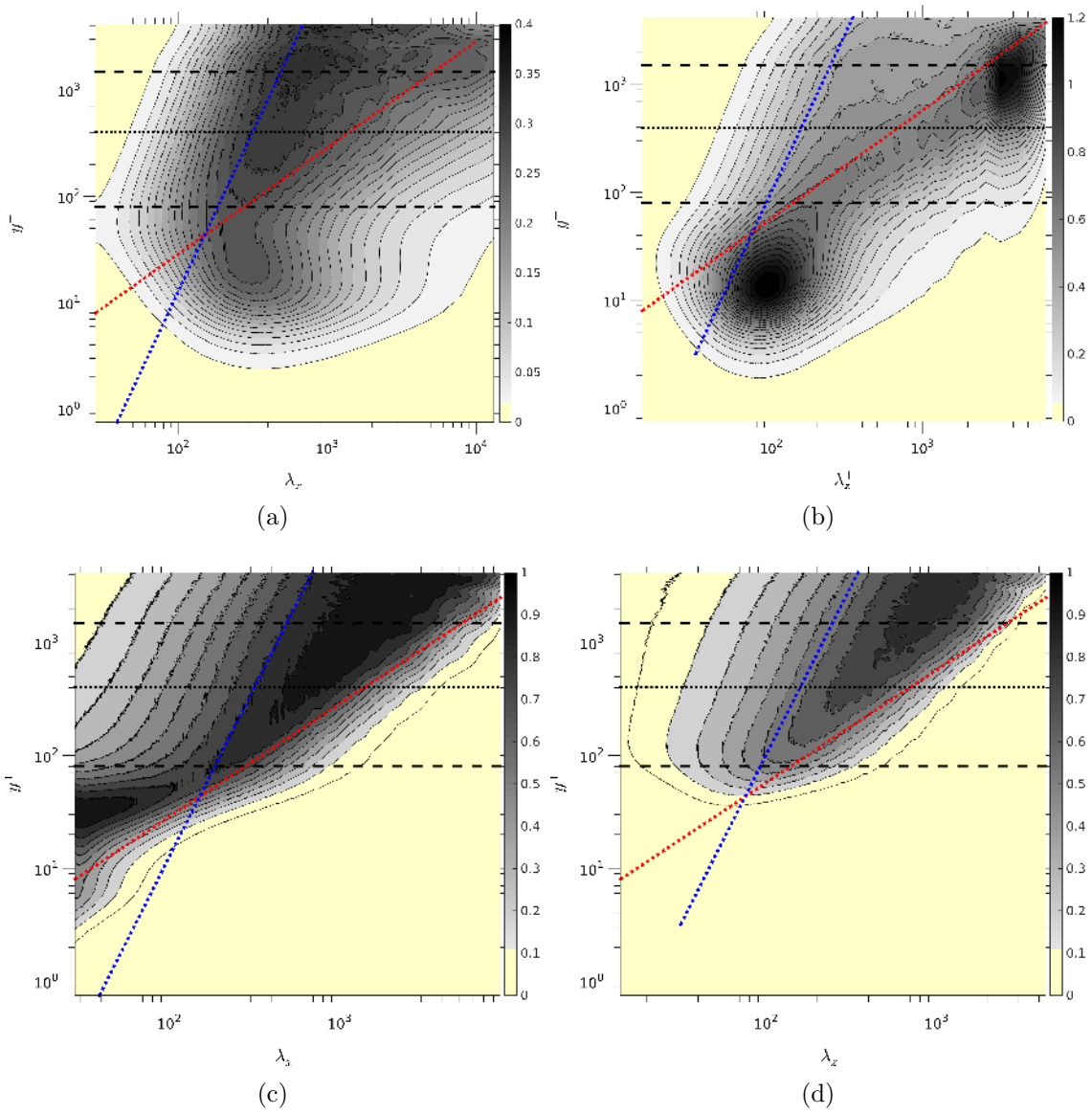

FIG. 3. Characterisation of isotropy across eddy-size range: (a) compensated spectra $\epsilon^{-2/3}k_x^{5/3}\Phi_{uu}$, (b) compensated spectra $\epsilon^{-2/3}k_z^{5/3}\Phi_{uu}$, (c) and (d) maps of the square of the "isotropy parameter" $(\gamma^{3c})^2$, derived from the streamwise and spanwise spectral components. The red lines show either the relation $\lambda_x^+ = 3.5y^+$ or $\lambda_z^+ = 7y^+ = 2\lambda_x^+$ and the blue lines show either the relation $\lambda_x^+ = 3.5(y^+)^{1/3}$ or $\lambda_z^+ = 7(y^+)^{1/3} = 2\lambda_x^+$.

that this peak in streamwise energy is associated with structures having wavelengths of order $\lambda_x^+ \gtrsim 8000$ and $\lambda_z^+ \gtrsim 4000$. The near-wall energy peak, at $y^+ \approx 10$ is also clearly brought out in the $(\gamma_u^{1c})^3$ maps, in which a maximum at $\lambda_z^+ \approx 100$ is evidently indicative of the strong small-scale streaks in the buffer layer.

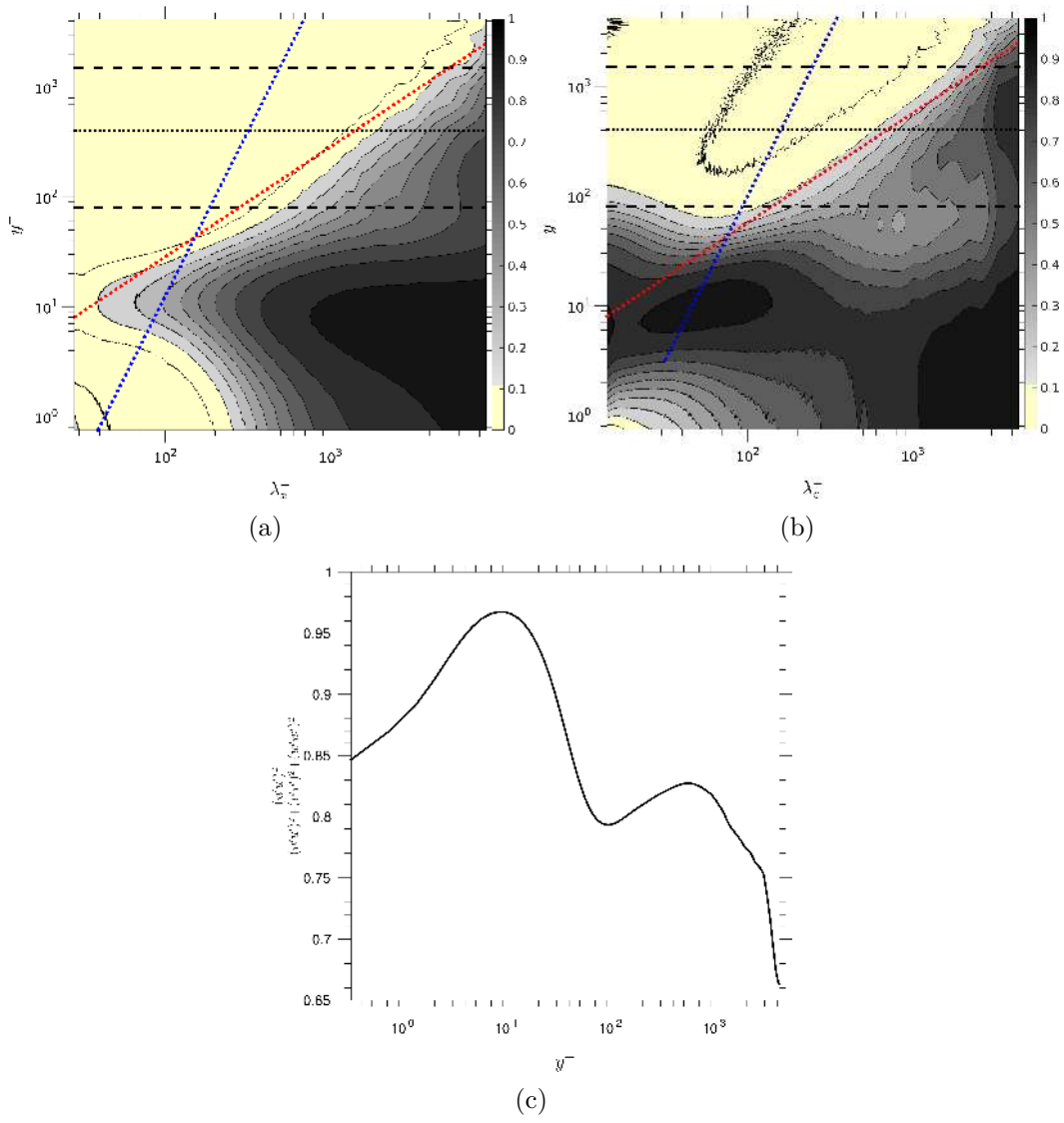

FIG. 4. Characterisation of anisotropy due to dominance of streamwise energy $\overline{u'u'}^+ >> \overline{v'v'}^+, \overline{w'w'}^+$: (a) maps of $(\gamma_u^{1c})^3$ in streamwise direction, (b) maps of $(\gamma_u^{1c})^3$ in spanwise direction and (c) cross-spectrum average of γ_u^{1c}. Red and blue dotted lines: see caption of figure 3.

C. Anisotropic Range – Small-Scale Motions

The maps shown in figures 3 and 4 contain small-scale ranges to the left of the blue lines $\lambda^+ \propto (y^+)^{\frac{1}{3}}$ which neither comply with isotropy nor with one-component dominance. The scales in question are not far from the Kolmogorov range $\lambda^+ \propto (y^+)^{\frac{1}{4}}$. In order to identify the state of the turbulence in this range, a third parameter, γ_{ij}^{2c}, is defined as follows:

$$\gamma_{ij}^{2c} \equiv \frac{2|\Phi_{ii}||\Phi_{jj}|}{|\Phi_{uu}|^2 + |\Phi_{vv}|^2 + |\Phi_{ww}|^2} \tag{4}$$

This parameter identifies the dominance of two normal components, $i \neq j$, over the third, and thus highlights the range where the anisotopic turbulence is characteristic of two-component turbulence. Figure 5(a) shows a map of $(\gamma_{vw}^{2c})^3$, which brings into focus the region where the spectra of the wall-normal and spanwise components have similar energy level, both exceeding the streamwise component. The suggestion emerging from this map is that small-scale motions, of scales λ_x^+ lower than $3.5 \times (y^+)^{1/3}$, are characterised by $\overline{v'_{ss}v'_{ss}}^+ \approx \overline{w'_{ss}w'_{ss}}^+ > \overline{u'_{ss}u'_{ss}}^+$. This rather unexpected result has motivated the isolation of these small scales from larger scales by means of a spatially two-dimensional version of the Empirical Mode Decomposition (EMD), previously used by Agostini & Leschziner[32–34] . The distinction between small and large scales is not precise, and it depends of the number of intrinsic modes (here 6) used for the separation process. Hence, in the present context, the separation is rather tentative. Nevertheless, the energetic properties of the small scales, shown in figure 5(b), support the implication of figure 5(a) to the extent that, above the buffer region, the wall-normal and spanwise small-scale energy components exceed the streamwise component. Attention is drawn to the $\sqrt{y^+}$ scaling of the energy components in figure 5(b), intended to bring to the fore the constancy of the scaled energy components, the magnitude of which thus varies as $1/\sqrt{y^+}$. The physical significance of the plateau region arising from the $\sqrt{y^+}$ scaling is unclear, at present.

An interesting feature in the small-scale range emerges upon scaling the power spectrum as $y\epsilon^{-1/3}k_x^{7/3}\Phi_{uu}$. The use of k_x scaling reflects the fact that the energy level in the spectrum tends to vary with $k_x^{-7/3}$ in anisotropic turbulence. When the y-scaling is added to the compensated spectrum, the resulting map, shown in figure 5(c), features an elongated plateau within the meso-layer, just to the left of the blue line $\lambda_x^+ = 3.5 \times (y^+)^{1/3}$. The implication is that the contribution of small-scale energy to the total energy declines inversely with y^+.

D. Summary of Sub-Ranges

Based on considerations so far, it is possible to identify distinct regions within the spectral map in which the structures possess different characteristics. Such a map is proposed in

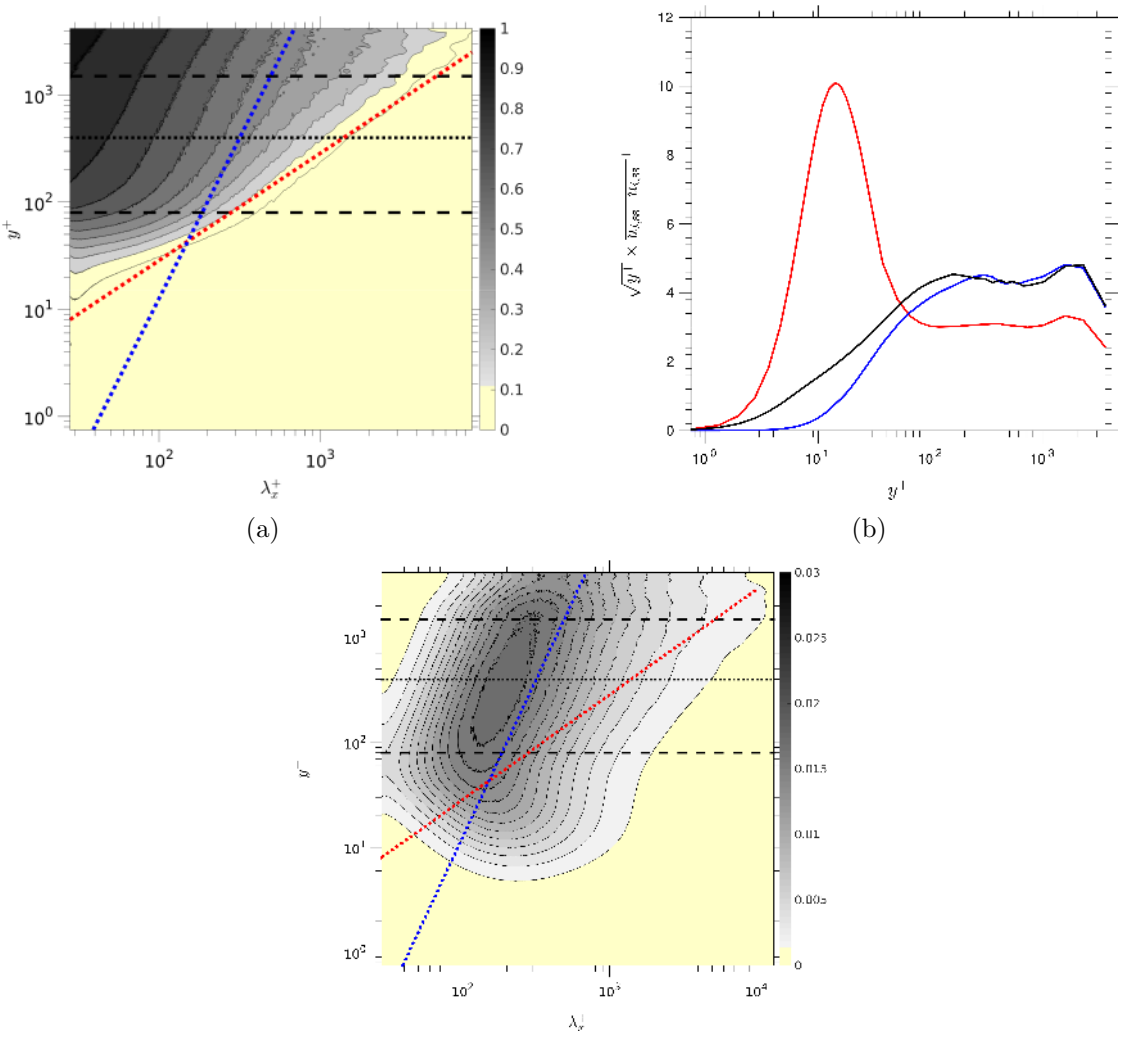

FIG. 5. Characterisation of anisotropy of small-scale motions due to dominance of cross-flow energy components: (a) map of $(\gamma_{vw}^{2c})^3$, (b) streamwise stress associated with small-scale motions, normalised by $\sqrt{y^+}$: streamwise stress (red line), wall-normal stress (black line) & spanwise stress (blue line), and (c) compensated power spectra $y\epsilon^{-1/3}k_x^{7/3}\Phi_{uu}$. Red and blue dotted lines: see caption of figure 3.

figure 6.

Within the meso-layer, of primary interest herein, there are three major regions:

- Region "A", associated with (very) small scales, is characterized by a dominance of the wall-normal and spanwise component over the streamwise fluctuations.

- Region "B" is characterized by a trend towards isotropy. This is, essentially, indicative of the inertial sub-range, where the eddies are presumed to be "detached".

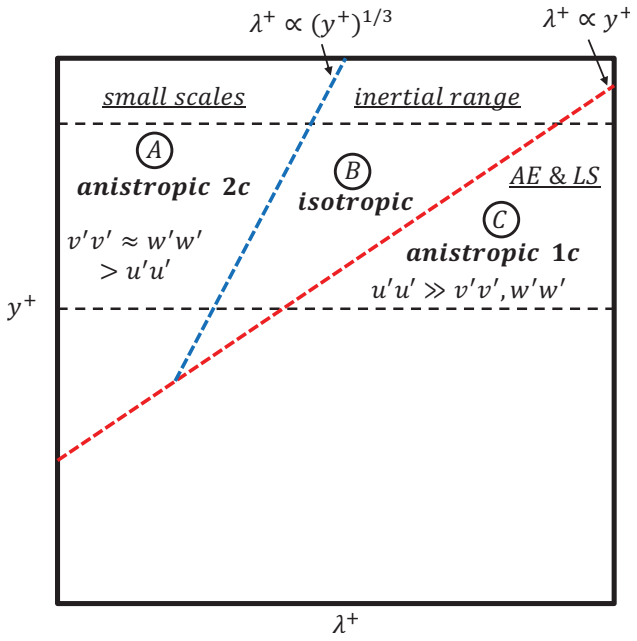

FIG. 6. Sub-ranges in spectral map having distinct turbulence characteristics (1c: dominance of streamwise component; 2c: dominance of cross-flow components).

- Region "C" is characterized by a high level of anisotropy in the scales, with the streamwise component dominating and the streamwise and spanwise components larger than the wall-normal component. This region is associated to the attached eddies and with large-scale motion. It is emphasized here that this region extends across the entire meso-layer. While the associated condition $\Phi_{uu} \propto k^{-1}$ is not clearly present in figure 2, an examination of the structure function, to follow, will support the interpretation of this region being associated with attached eddies.

III. THE ATTACHED EDDY HYPOTHESIS

A. Structure-Function Analysis

In the absence of a clear region of $\Phi_{uu} \propto k^{-1}$, conventionally associated with the Townsend-Perry AEH, attention is directed towards the second-order structure function $S_{2,u}(y, \delta)$ as a potentially superior indicator of the validity of the AEH. This is a route previously advocated by Davidson et al.[6,7]. Its rationale is based on the observation that there is a close correspondence between the pre-multiplied spectra and the derivative of the second-order structure function. In particular, Davidson et al argue that, since the two are

effectively Fourier-transform pairs, the structure function should exhibit a real space analogue of the k^{-1} spectrum, shown to manifest itself by a constant value of the pre-multiplied derivative of the structure function. This correspondence is pursued and exploited below.

In channel flow, with homogeneous directions x and z, the relevant second-order structure functions are:

$$S_{2,u}(y,\delta_x) = \left\langle \left[u\left(y,x\right) - u\left(y,x+\delta_x\right)\right]^2 \right\rangle_{z,t} \qquad (5)$$
$$S_{2,u}(y,\delta_z) = \left\langle \left[u\left(y,z\right) - u\left(y,z+\delta_z\right)\right]^2 \right\rangle_{x,t}$$

with the subscripts at the end identifying the averaging directions.

The structure function essentially represents the total energy contained within the range of eddies with size less or equal to δ (either δ_x or δ_z). The contribution from eddies larger than δ is negligibly small, because $u\left(y,x\right) \approx u\left(y,x+\delta\right)$. When $\delta = L$, the largest distance across which there is a correlation between motions at x and $x+\delta$, i.e. with the motions uncorrelated, $S_{2,u}(L)$ reaches a maximum equal to twice the streamwise turbulence energy. At the other extreme, $\delta = 0$, $S_{2,u}(0) = 0$, and the correlation reaches a maximum.

The contribution to the energy associated with eddies having a length δ is given by the pre-multiplied derivative of the structure function (PMDS2) $\delta \times \frac{dS_{2,u}(\delta)}{d\delta}$ (Townsend[1], Davidson at al.[6]). This is equivalent to, but not the same as, the premultiplied power spectra ($k\Phi_{uu}$) . Given a constant level of the PMDS2, which is consistent with a k^{-1} variation of the spectrum (Davidson et al), integration then immediately yields a logarithmic variation of $S_{2,u}(\delta/y)$ and thus a logarithmic dependence $\overline{u'u'}^{+}(\delta/y)$ for $\delta = L$. In summary then: there is a mutually consistent linkage between a k^{-1} spectrum, a constant level of the PMDS2, the logarithmic variation of $\overline{u'u'}^{+}$ and the AEH. It is not surprising, therefore, to observe a striking similarity between the pre-multiplied power spectra and the corresponding PMDS2, as emerges upon comparing the maps in figures 7(c) and (d) with those in figure 2.

Attention is drawn to the fact that the scaling adopted for the abscissa in the x-wise and z-wise maps in figure 7 are $8\delta_x$ and $4\delta_z$, respectively. A consequence of including the multipliers 8 and 4, respectively, is that the range of values covered in figure 7 corresponds closely to those in figure 2. This might seem an arbitrary argument, but there is also some rational justification for it. This emerges upon a closer examination of the relationship between the

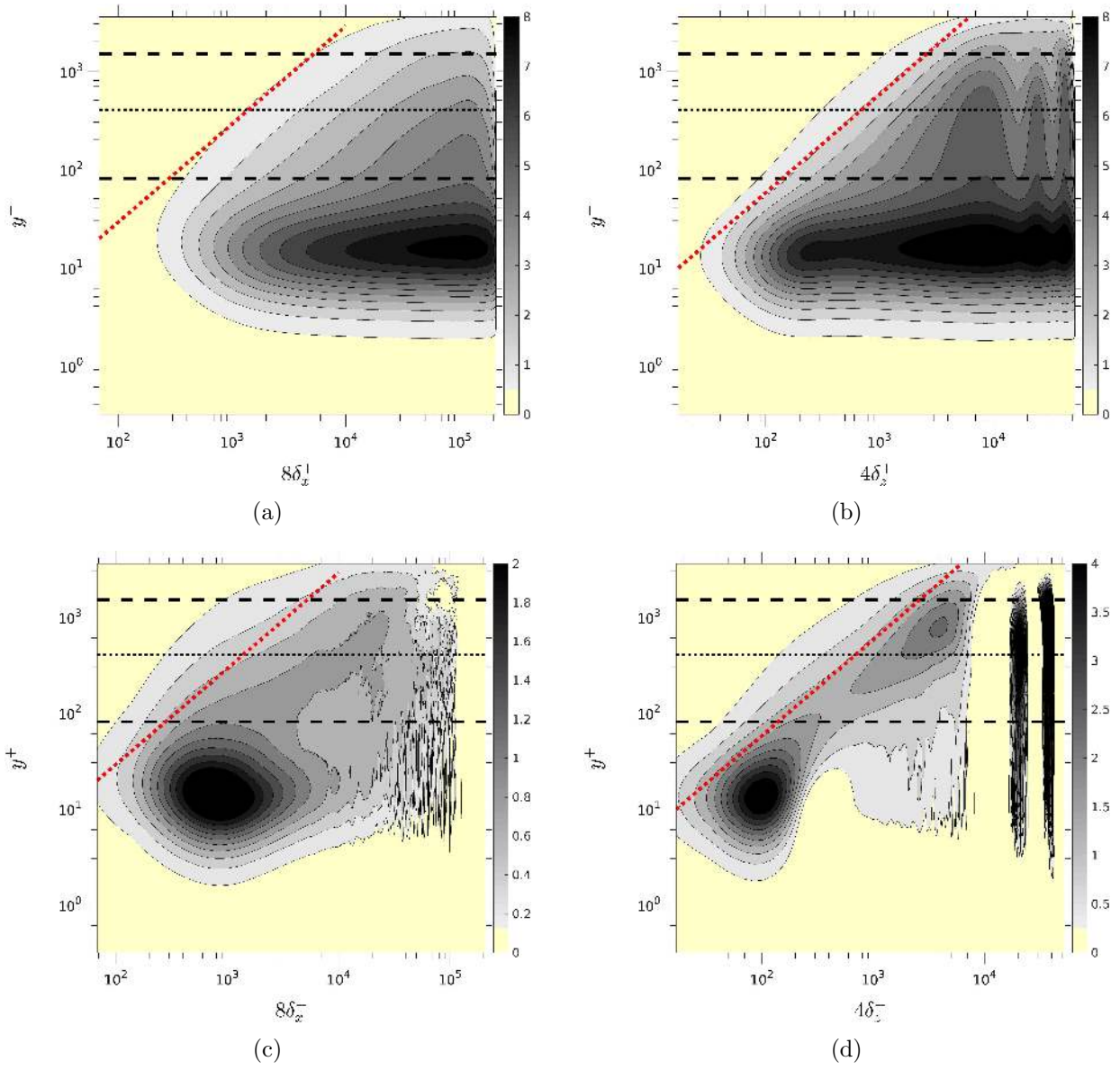

FIG. 7. Maps of the second-order structure function and its pre-multiplied derivatives:(a) $S_{2,u}(\delta_x)/2$; (b) $S_{2,u}(\delta_z)/2$; (c) $\delta_x(dS_{2,u}/d\delta_x)$; (d) $\delta_z(dS_{2,u}/d\delta_z)$. Red and blue dotted lines: see caption of figure 3.

spectra and the structure function, subject to idealised conditions. Such an examination is presented Appendix A, for two idealized ("toy") conditions. One key relationship that emerges from the considerations in the Appendix is that the spectrum is related to the derivative of $S_{2,u}$ by:

$$\frac{dS_{2,u}(\delta)}{d\delta} = 2\frac{d}{d\delta}\left[\int_0^{+\infty} \cos(k_x\delta)\Phi_{uu}(k_x)dk_x\right] \tag{6}$$

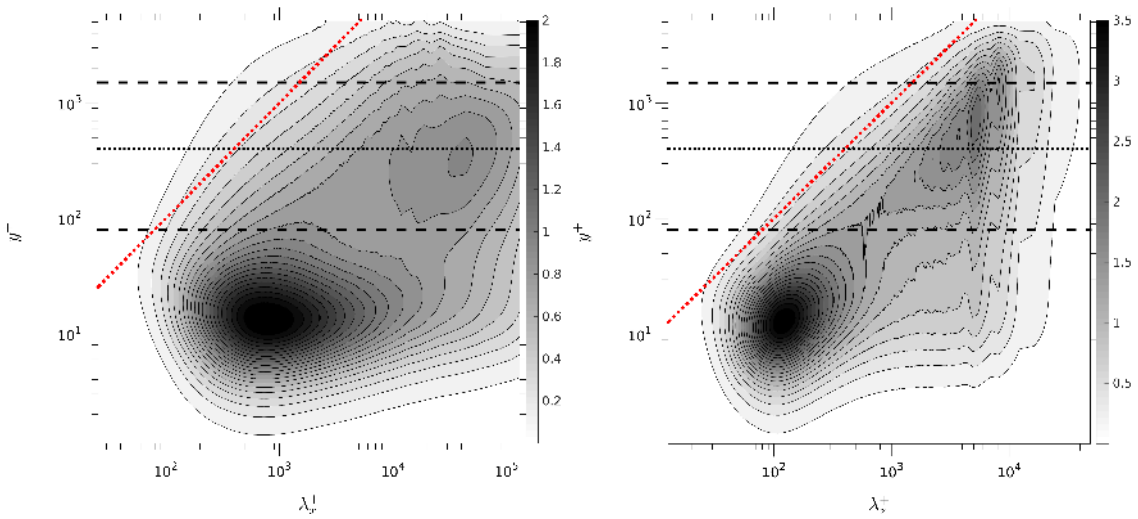

(a) (b)

FIG. 8. Pre-multiplied power spectra of the streamwise fluctuations for $Re_\tau = 5200$ derived from data by Lee & Moser[28]; (a) streamwise spectra; (b) spanwise spectra.

It is this relationship that forms the basis for examining the two toy representations of ϕ_{uu} and the corresponding derivative of the structure function. In particular, a mono-chromatic (with $\lambda = \lambda_{x_0}$) and a 4-wave-number (with $\lambda_{x_i} < \lambda_{x_0}$, for $i = 1, 2$ and 3) representations of $u(x)$ are examined, and these are argued to imply that the relation between δ and λ is $\delta = \lambda_{x_0}/4$ for a mono-chromatic signal, with the constraint $k\Phi_{uu} = cst$ the ratio dropping with increasing number of modes .

As is recognised upon comparing figure 2(b) with figure 7(d), the contours in the PMDS2 matches those in the corresponding pre-multiplied spectrum if δ_z is multiplied by a factor 4 in the former map. The eddies may thus be associated with a monochromatic signal. In the log-law region, for $4\delta_z \lesssim 5 \times 10^3$, the wall-normal distribution of the locus of the maximum value follows the relation $\delta_z^+ \propto y^+$, whatever the y-locations, the increase towards the maximum value being monotonic. Hence the energy is associated mainly with eddies of a particular size $\delta_{z,o}$, which increase with y. If, in contrast, the "coherent" structures are described by a range of Fourier modes (with $\lambda \leq \lambda_{x_0}$), the qualitative trend is for the ratio 1/4 to decrease, as demonstrated in the Appendix. In this case, at $\delta = 0$, the curvature of $S_{2,u}(\delta)$ depends of the frequency content of the signal: it strengthens if the signal is associated to a wide range of frequency (Townsend[1]). This applies to the spectra and structure-function maps in the streamwise direction. Thus, a match between the corresponding maps in the streamwise

direction, figure 2(a) and figure 7(c), is obtained if δ_x is multiplied by 8 in the latter map.

The PMDS2 maps conveyed by figures 7(c) and (d) ($\delta_x dS_{2,u}/d\delta_x$ and $\delta_z dS_{2,u}/d\delta_z$, respectively) show a number of features that are absent or not clearly delineated in the spectra.

First, the range of useful resolution in terms of δ_x exceeds that offered in terms of λ_x. This is simply a consequence of tighter limitations on the post-processing yielding the spectra.

Second, and associated with the first, these figures suggest the presence of spanwise spatial quasi-periodicity in the very large scales, at the extreme right of the map of $S_{2,u}(y, \delta_z)$ (figure 7(b)), where an oscillatory pattern at two distinct wavelengths is visible, both also displaying strong wall-normal coherence. These are not captured by the spectra, because of convergence limitations at large wavelengths associated with the relatively small simulation domain. As noted in the Appendix, S_2 is closely associated with the correlation function. Hence, the oscillatory pattern suggests the presence of spanwise-correlated motions. However, in view of the rather small box size (especially πh in the spanwise direction), the question might be posed as to whether the oscillatory behaviour seen in figure 7(b) and the associated bands in figure 7(d) are physically significant.

One part of the answer rests on the observation that the oscillatory behaviour arises at $\delta z^+ \approx 5000$ (i.e. $\approx h$) and 10000, the former value being substantially lower than the spanwise domain size $L_z^+ = 13000$. There is reason, therefore, to suppose that at least the shorter wave-length feature is physically significant, reflecting the spanwise quasi-periodicity of large-scale motions and their footprints, observed by Agostini & Leschziner[32] to be separated by a distance of order h at $Re_\tau = 1020$.

Support for the above argument is offered by the spectra shown in figure 8 for $Re_\tau = 5200$, obtained from the limited amount of the DNS data available for the large-box simulation of Lee & Moser[28]. The spanwise spectral map is seen to contain spectral bands at $\lambda_z^+ \approx 5000$ and 8000, which support the supposition that the bands in figure 7(d) reflect a physical process. There are no such features beyond $\lambda_z^+ \approx 10000$.

Third, the seemingly "noisy" portions present in these maps at low y^+ and intermediate δ values are argued to constitute a physical feature and reflects the fact that medium-scale motions are strongly correlated across the near-wall layer, and are present on top of earlier mentioned large-scale footprints associated with outer large-scale motions in the upper portion of the meso-layer.

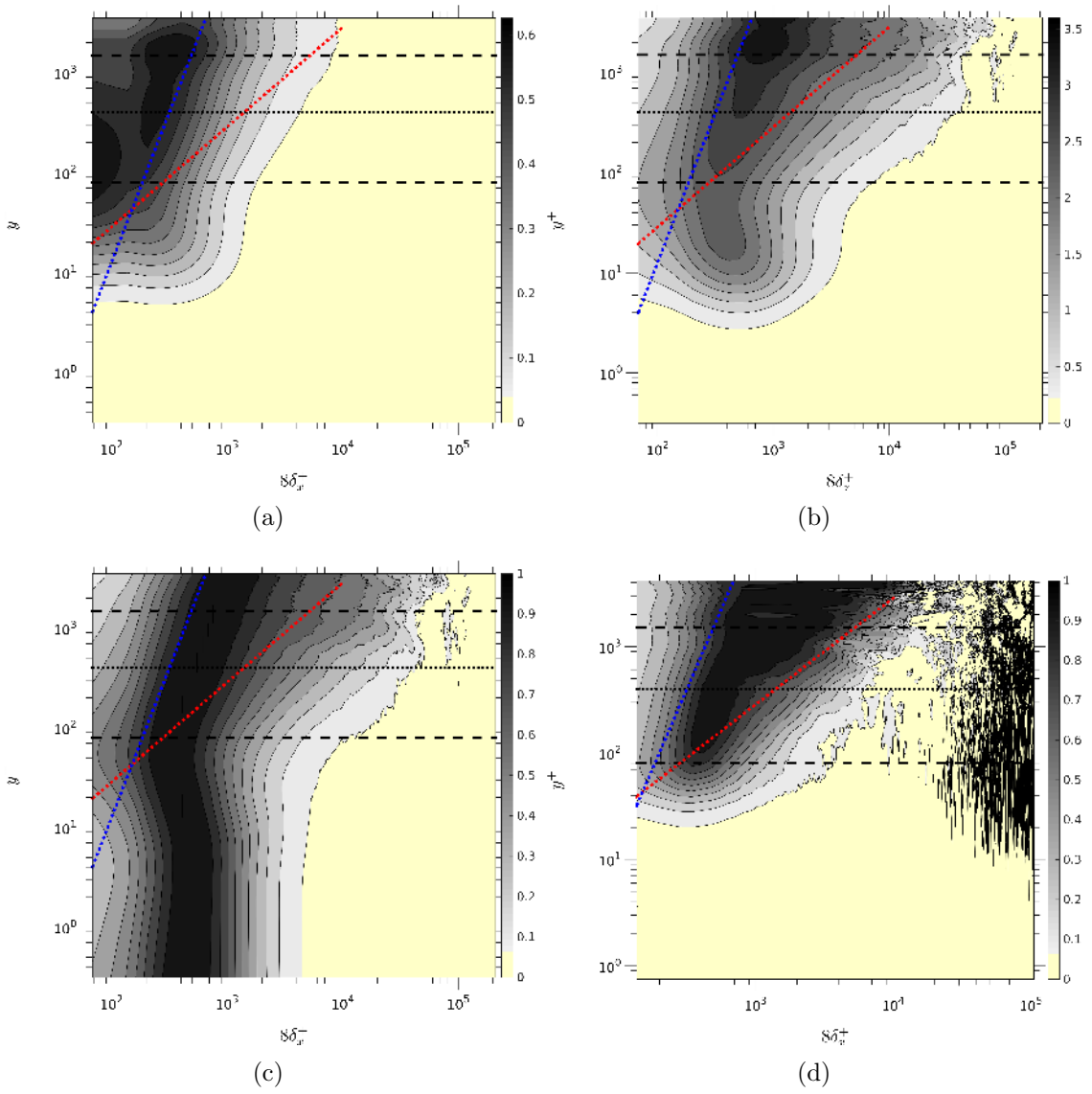

FIG. 9. Turbulence state, premultiplied derivative of the structure function compensated by : (a) $\epsilon^{-1/3}\delta_x^{-4/3}$, (b) $\epsilon^{-2/3}\delta_x^{-2/3}$; (c) the compensated $\delta_x \frac{dS_{2,u}}{d\delta_x}$ defined for the isotropic case is divided by the maximum value at each y-location and (d) isotropic parameter $(\gamma^{3c})^2$. Red and blue dotted lines: see caption of figure 3.

B. The Regime of Attached Eddies

Following Townsend[1] and Davidson et al.[6,7], among others, the PMDS2 may be used to shed light on the validity of the AEH. The relevant test is whether $\delta dS_{2,u}/d\delta = cst$[1,7].

In Section II D, it was proposed that the meso-layer may be divided into three physically different domains - A, B and C in figure 6. These are associated, respectively, with spectra of the form $\phi_{uu} \sim \epsilon^{1/3}k_x^{-7/3}$, $\phi_{uu} \sim \epsilon^{2/3}k_x^{-5/3}$ and $\phi_{uu} \sim k_x^{-1}$, the last indicative of the AEH.

As argued by Pope[35], a power-law spectrum $\Phi(\omega) \approx C_1\omega^{-p}$ can be related to the second-order structure function $S_p(\delta) \approx C_2\delta^q$ with $p = q + 1$, valid only under the condition that $p > 1$. In accordance with the AEH, $p = 1$, in which case Davidson et al.[6,7] show that $S^2(\delta) \approx C_3 \log(\delta) + B$. The implications for subregions A, B and C in figure 6 are therefore, respectively:

- region A: $\delta_x dS_{2,u}/d\delta_x \sim \epsilon^{1/3}\delta_x^{4/3}$
- region B: $\delta_x dS_{2,u}/d\delta_x \sim \epsilon^{2/3}\delta_x^{2/3}$
- region C:, $\delta_x dS_{2,u}/d\delta_x = cst$

Figure 9(a) shows a map of $\delta_x \frac{dS_{2,u}}{d\delta_x}$ compensated by $\epsilon^{-1/3}\delta_x^{-4/3}$. As expected, on the basis of the above statements on the spectra, there is a "plateau" in region A, bounded by the blue line. Figure 9(b) relates to the isotropic state through the augmentation by $\epsilon^{-2/3}\delta_x^{-2/3}$, along with a normalized version thereof in figure 9(c), in which the levels at any y-value are normalised by the maximum at that level. Both maps bring to light the plateau in region B in the meso-layer, bounded by the blue and red lines. This region is narrow in the lower part of the layer, but broadens as y increases – i.e. the inertial range becomes wider in the outer portion of the log-layer. These features concur with those in the map in figure 4 showing the parameter $(\gamma^{3c})^2$ (see equation 2). The PMDS2 maps shown in figure 7(c) and (d) – especially the latter – include an oblique band to the right of, and parallel to, the red line, i.e. region C, in which the condition $\delta_x dS_{2,u}/d\delta_x = cst$ is met, at least approximately. Although this provides some support for the validity of the AEH in the meso-layer, the absence of a well-defined plateau is counter-indicative. Further support is sought, therefore, from an examination of joint PDFs pursued below. Implicit in this route being taken is the assumption that the processes in the spectral range C dominates over those in ranges A and B, assumed to make sub-ordinate contributions to cross-scale-averaged PDFs.

In an effort to shed light on any statistical bias in the motions within the meso-layer, and thus possibly draw inferences on the "shape" of the coherent structures, attention is directed first towards the skewness of the PDFs in the meso-layer. Figure 10(a) shows the wall-normal distributions of skewness of the streamwise fluctuations and their streamwise derivative. The inclusion of the latter, in combination with the former, may be argued to allow observations to be made on a streamwise bias in the length scales, which then

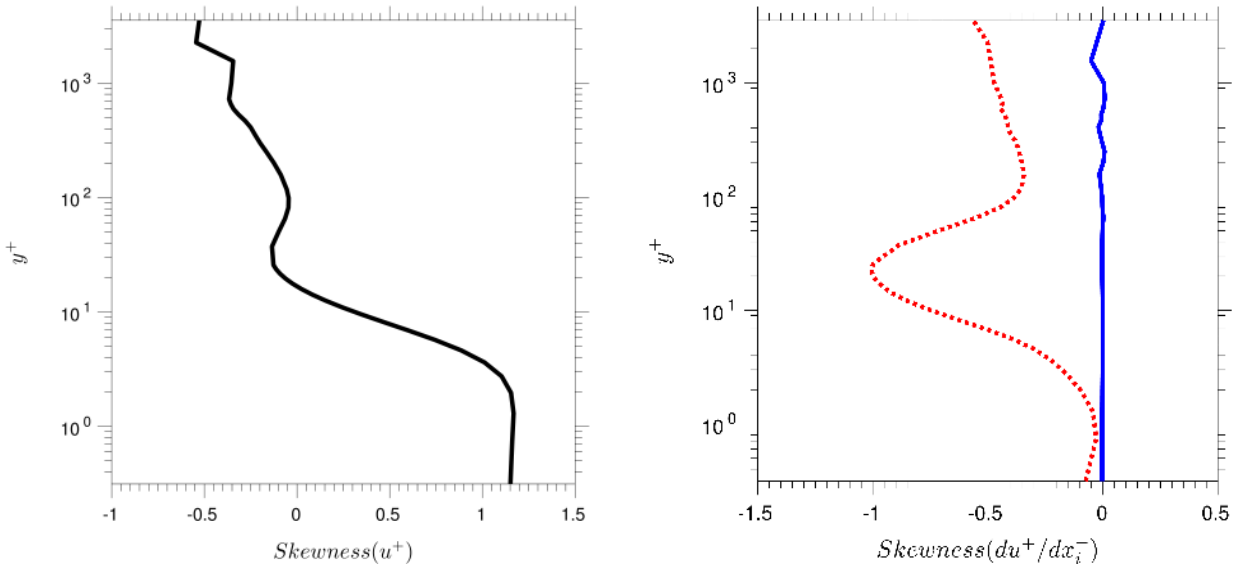

FIG. 10. Wall-normal distribution of: (a) the skewness of the streamwise velocity, (b) the skewness of the streamwise and spanwise derivative of the streamwise velocity, identified by the red and blue lines, respectively.

leads to statements on the shape of the coherent structures. Both figures bring to light a substantial asymmetry in the streamwise fluctuations: few large negative events occurring in combination with many weak positive events. This also suggests asymmetric structural properties of the coherent motions, an issue pursued next by reference to joint PDFs of the streamwise fluctuations and their derivatives.

Figures 11(a) and (b) show, respectively, joint u^+-du^+/dx^+ and u^+-du^+/dz^+ PDFs at $y^+ = 600$, a position approximately in the middle of the meso-layer. Conclusions derived for this position apply across the entirely meso-layer, as the level of skewness levels of the PDFs for the velocity fluctuations and their streamwise derivative are fairly uniform. Figure 11(a) reveals three major features: first, consistent with the skewness level in figure 10(a), there is a distinct asymmetry in the u^+-fluctuations field; second, weak positive fluctuations occur in combination with high negative du^+/dx^+ values, from which it can inferred that the length scale of the positive fluctuations is relatively small; third, strong negative fluctuations occur in combination with low values of positive du^+/dx^+, suggesting relatively large length scales; fourth, negative values of du^+/dx^+ tend to be larger than positive ones, in line with the skewness level in figure 10(b). There is, therefore, a bias in the length scales associated with deceleration and acceleration, with the latter less numerous, but more in-

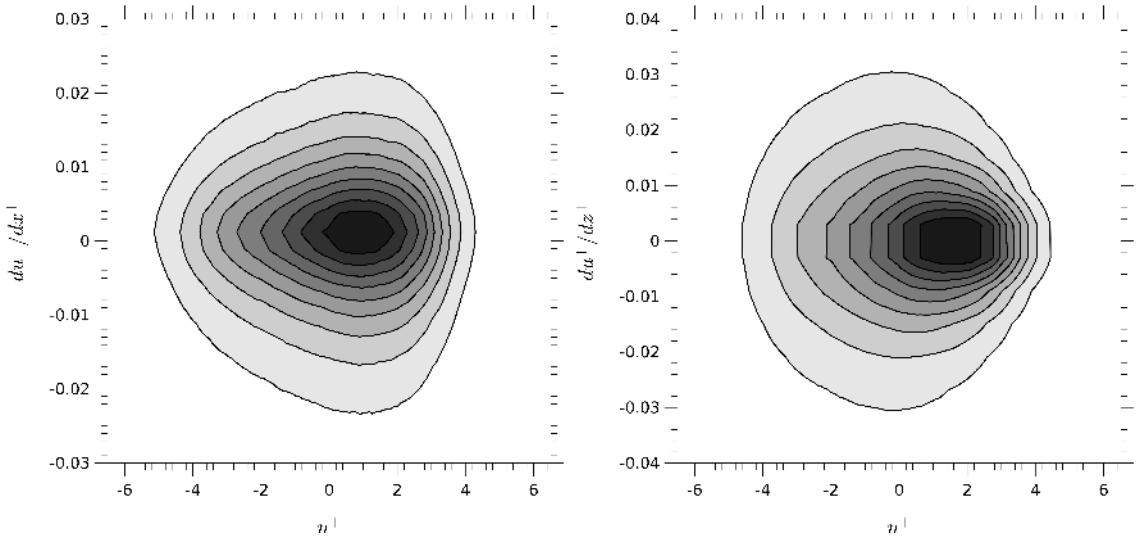

(a) (b)

FIG. 11. Joint PDFs between the streamwise velocity and its derivative at $y^+ \approx 600$: (a) u^+-du^+/dx^+ and (b) u^+-du^+/dz^+. PDF contours identify 0.10.9 of the PDF height at constant increment 0.1, subject to total PDF volume normalized to 1.

tense. In figure 11(b), it is observed, first, that the contours of du^+/dz^+ are symmetric. This concurs with the zero-skewness line of the PDFs of du^+/dz^+ in figure 10(b). Second, and in contrast to the PDF in figure 11(a), large spanwise gradients occur in combination with negative u^+-fluctuations, while low spanwise gradients occur in combination with high velocity fluctuations. Again, interpretation of these combinations as conveying information on the length scale, it may be inferred that the spanwise length scale is relatively large in combination with positive fluctuations and relatively small in combination with negative fluctuations.

The skewness distributions, and the length scales inferred, qualitatively, from the joint PDFs in figure 11 and the ratio between λ and δ previously argued, suggest the form of "coherent structures" conveyed conceptually in figure 12. This structure, symmetric in the spanwise direction and tail-like in the streamwise direction, arguably provides support for the AEH. In particular, it is consistent with the sequence of several generations of attached eddies, as indicated in the sketch.

Further evidence in support of the AEH is provided by features contained in the maps of the PMDS2, figures 7(c) and (d). These maps are reproduced in figures 13 and 14, in which two regions are highlighted: a blue triangular region and a more restricted red trapezoidal

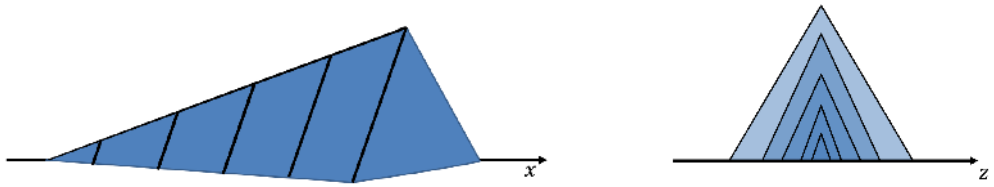

(a) (b)

FIG. 12. Conceptual sketch of the "form" of the coherent structures associated with attached eddies.

region, both covering the meso-layer.

If a perfect plateau in the PMDS2 and the corresponding pre-multiplied spectra existed within the triangular region, the implications regarding the AEH would be those shown in schematic 13. In this conceptual representation, e_i are representative attached eddies. Notional y-wise variations of the eddies' respective energy contributions $\overline{u'u'}^+$ and scaled variations thereof, with the scaling variables being the eddy height (h) and wave length (λ), are shown alongside the conceptual attached-eddy sketch. The collapse in the scaled uniform profiles reflects the linear dependence of the eddy height on y and the implied constancy of $k\Phi_{uu}$ in the premultiplied spectra. This is then fully consonant with the AEH and also with logarithmic variation of $\overline{u'u'}^+$ expressed by equation 1.

As is evident from figure 7, there is no clear plateau within the triangular region, probably because the Reynolds number is low. However, there is an approximately constant level within the red trapezoidal region. One consequence of this restricted plateau region is that the logarithmic variation in equation 1 only applies in the upper portion of the meso-layer, above the dotted line in figures 7(c) and (d). Below that line, the linear variation of the parallel boundaries of the trapezoid, when transcribed to the pre-multiplied spectra, implies a constant level of $\overline{u'u'}^+$, broadly in line with the variations shown in figure 1.

The restricted plateau region in the trapezoidal region leads to the interpretation shown in figure 14. Prior to this interpretation, however, figure 13 provide the conventional view introduced by Townsend, as a background against which to discuss figures 14.

The sketches in figure 13(b)-(d) show a sequence of four attached eddies, $e_1 - e_4$, whose energy rises with height such that the eddies collapse if the energy density and height are normalised by $\lambda = 1/k = y$ - i.e., the eddies are self-similar. If these eddies exist in the triangular region of the spectrum, within which $k\Phi_{uu} = cst = A$, limited between $\lambda_{min} = y$ and $\lambda_{max} = cst$, as shown in figure 13(e), it follows that the energy $\overline{u'u'}$ varies logarithmically with y, as shown in figure 13(f), which arises from equation 1. The implication is thus that, at any y-location, only eddies larger than the attached eddy at that height contribute to the energy, and that all such eddies contribute at the level $k\Phi_{uu} = A$.

Figure 14 now pertain to the trapezoidal domain shown in figure 7. The upper part of this domain is triangular, which thus conforms to the relationship shown in figure 13. Figures 14(b)-(e) relate to the parallelogram below the triangular region, with sketch (e) being an idealised representation of the profiles in sketch (b). As before, the normalisation $k\Phi_{uu} = A$ applies, but only over a restricted height of the eddies. Below the height defined by the lower line of the parallelogram $\lambda_{max}(y)$, the energy of the eddy declines rapidly – notionally, in a step-change manner to zero, as indicated by the transition between the two sketches 14(b) and (e). If, next, $\overline{u'u'}(y)$ is evaluated by integration between the parallel lines $\lambda_{min}(y)$ and $\lambda_{max}(y)$ – the lines bounding the parallelogram (see figure 14(f)) the result is a plateau of $\overline{u'u'}$, as shown in figure 14(g).

This representation differs substantially from the conventional AEH, but does imply a self-similar set when scaling with h and λ is effected. It is thus arguable that the plateau region within the trapezoidal region in figures 7(c) and (d) is fundamentally consistent with the AEH even though there is no clearly defined triangular plateau region. This interpretation also explains the plateau in the $\overline{u'u'}$ profile.

As an aside, although relevant to the above argument, it is interesting to consider the consequence of the Reynolds number being increased. On the assumption that the trapezoidal area is maintained, the change with the Reynolds number leads to the blue region in figure 15 changing to the red area, subject to $\lambda_{min}(y)$ remaining invariant. The consequence is then an increase in the plateau of $\overline{u'u'}$ and an extension of the logarithmic decline in $\overline{u'u'}$, as observed by Smits et al.[27], Hultmark et al.[14,25], Vallikivi et al.[36] among others.

Observations that give added support to the above arguments linking the AEH to the trapezoidal plateau region arise from averaging over a restricted segment of the DNS data, following the transient phase and covering approximately two global eddy-turnover periods

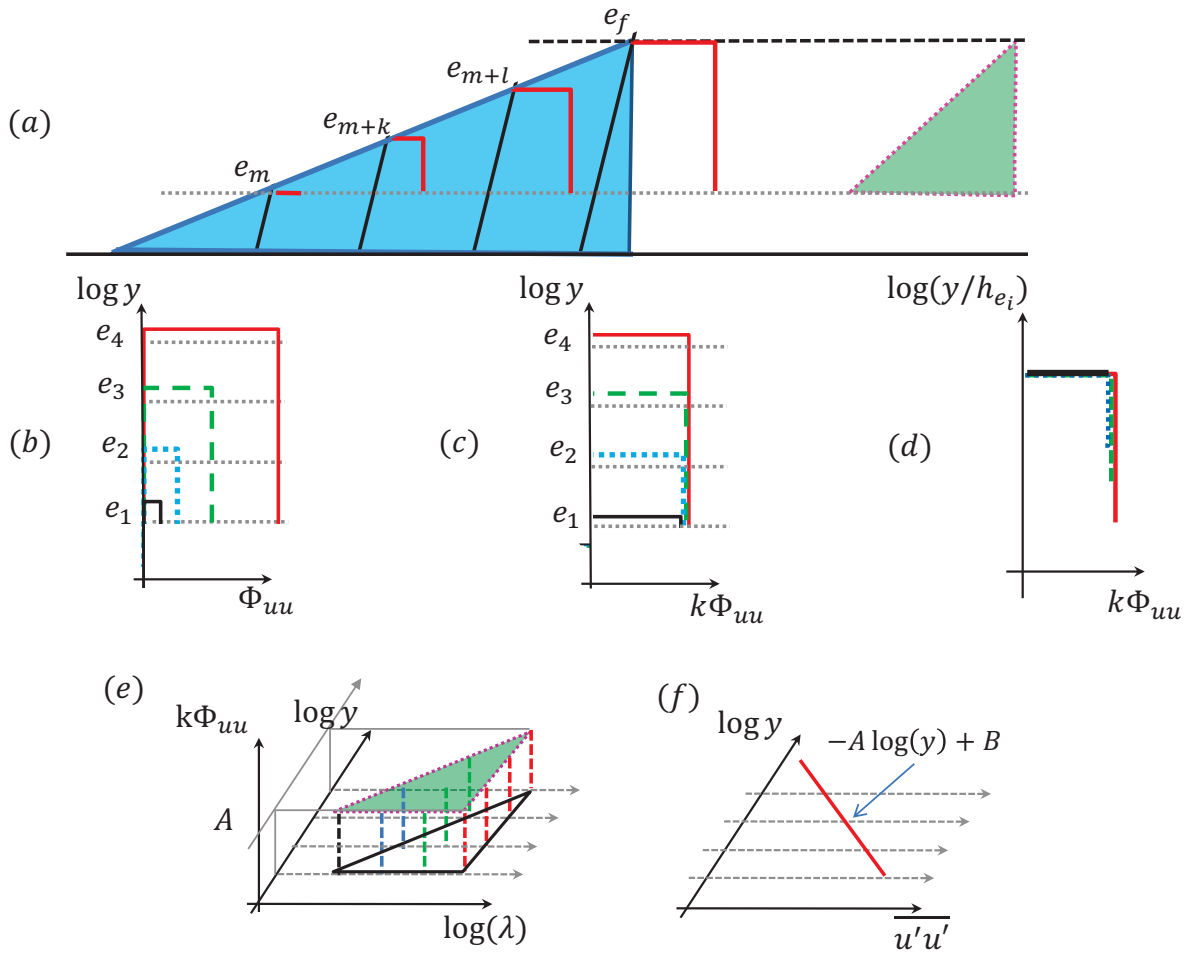

FIG. 13. Conceptual representation of the conventional Attached Eddy Hypothesis pertaining to a triangular plateau region in the spectrum or PMDS2 map: (a,b) hierarchy of attached eddies e_m, e_{m+k}, etc.; (c) eddy energy density normalized by λ; (d) eddy size normalized by h_{e_i}; (e) normalized eddies in the triangular plateau region; (f) resulting logarithmic profile of streamwise turbulence energy.

within the interval $2800 \leq t^+ \leq 3150$. It is emphasized here that this is done merely in order to add support to the validity of the relationship between the plateau in the trapezoidal area in figure 14 and the logarithmic decline of $\overline{u'u'}^+(y^+)$ in the meso-layer. The principal consequence of this restricted averaging is that the influence of the large-scale motion in the outer part of the log-layer on the statistics is reduced relative to averaging over the full duration of the simulation; the outer large-scales motions are observed to strengthen over the simulation period.

Maps of PMDS2 for the restricted interval are shown in figures 16(a) and (b), while the variation of the related streamwise-energy component is shown in figure 17. Upon comparing these maps in figure 7(c) and (d), it is immediately apparent that the nearly constant level

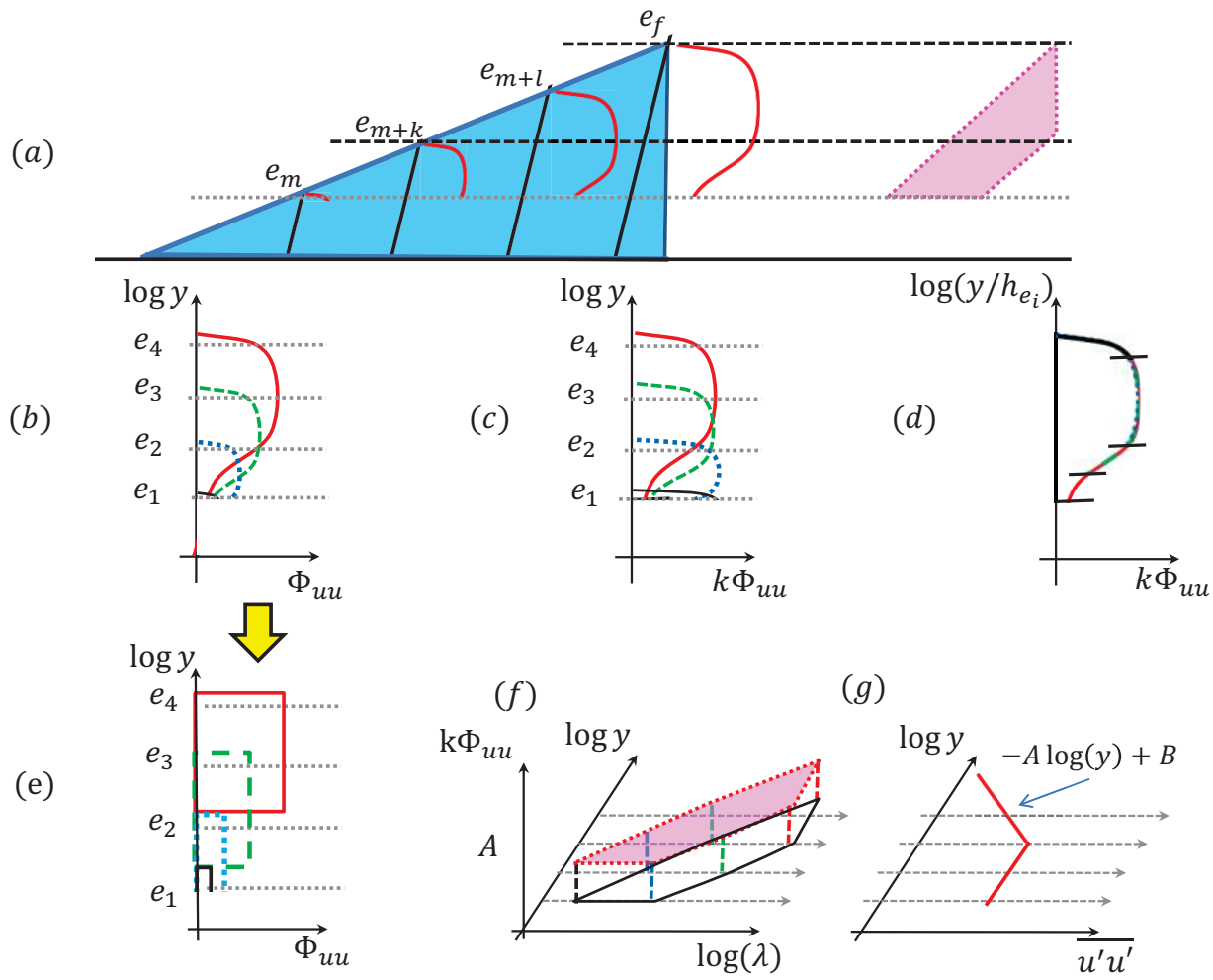

FIG. 14. Conceptual representation of the modified Attached Eddy Hypothesis pertaining to the trapezoidal plateau region in the spectrum or PMDS2 map: (a,b) hierarchy of attached eddies e_m, e_{m+k}, etc.; (c) eddy energy density normalized by λ; (d) eddy size normalized by h_{e_i}; (e) idealized representation of the energy density profiles in sketch (b); (f) normalized eddies in the trapezoidal plateau region; (g) resulting logarithmic and constant portions in profile of streamwise turbulence energy.

within the trapezoidal area – the plateau region – is far more pronounced in the former than in the latter. This is accentuated by the δ_x- and δ_z-wise profiles of the PMDS2, at different y^+ levels within the meso-layer, shown in figures 16(c) and 16(d), respectively. The profiles in the latter plot, in particular, feature a nearly constant level across the diagonal band contained within the trapezoidal region in figure 14. Based on the previously discussed relationships between the spectra, the PMDS2, and the log-law in figure 17, the expectation is that the levels of both plateau regions in 16(c) and 16(d) would be 1.26. This value is reasonably well returned in the streamwise-scale map, but is higher in the spanwise-scale

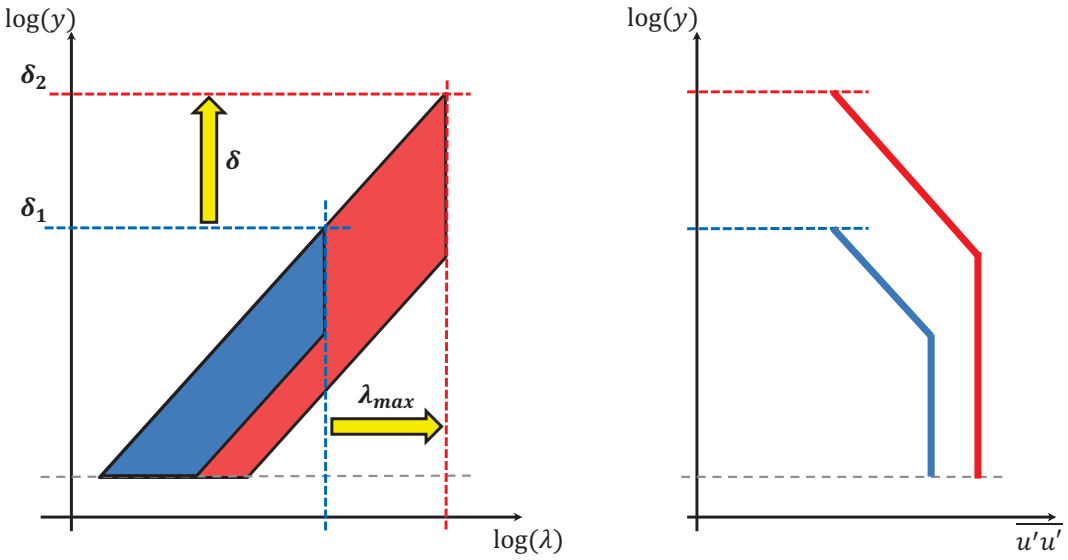

FIG. 15. Conceptual representation of the consequences of increasing Reynolds number: (a) enlargement of trapezoidal plateau region; (b) increase in the streamwise-energy plateau and wall-normal extension of the logarithmic region.

map. It is noteworthy that the differences between the two PMDS2 maps are mirrored by similar differences in the spectra both at $Re_\tau = 4200$ and 5200. While the origin of the difference is difficult to identify unambiguously, an issue that may play a role is that the spanwise eddy scales are constrained relative to the streamwise scales by the presence of wall-normal confinement. This is in contrast to unconfined boundary layers. As eddies evolve, wall-normal growth is inhibited, and energy is 'piling up' in eddies whose spanwise separation has to scale with h. This is not the case, however, in respect of streamwise scales, which can grow without inhibition.

Figures 16(e) and 16(f) confirm two observations made previously by Davidson et al[6,7], albeit only in respect of the streamwise scales and for a much narrower range of y^+. First, at any y^+, the increase in the structure function with δ^+ is logarithmic; second, the profiles collapse reasonably well when δ is scaled with y^+. This behaviour is, again, compatible with the AEH.

Consistent with the above features, the logarithmic decay of $\overline{u'u'}^+$ in the upper portion of the meso-layer $400 < y^+ < 1200$, shown in figure 17, is considerably more pronounced than in the corresponding profile in figure 1. In this range, $\overline{u'u'}^+$ follows $A \log y^+ + B$ with $A = 1.26$ and $B = 12.2$. Based on the AEH, Perry et al.[3] show that the constant A must be universal and that B depends of the large-scale motions. As shown by Hultmark et al[25],

Marusic et al.[13], Vallikivi et al.[36] and Chung at al.[9], in pipe flow and turbulent boundary layers, the value of the Townsend-Perry constant A lies in the interval 1.24-1.26.

A final observation made here on the PMDS2 map in figure 16(b) relates to the presence of four "fingers" in the sublayer, emanating from the region above it. These appear to be footprints of structures present in the meso-layer. Remarkably, they are equi-distant in log units, indicating a sequential doubling in the eddy size, which is in agreement with Perry et al's paradigm.

IV. SUMMARY AND CONCLUSIONS

The availability of DNS data for channel flow at the credibly high friction Reynolds number of 4200 has provided a rewarding foundation for exploring open questions on structural and spectral properties of near-wall turbulence. The examination has been undertaken by reference to maps of properties in the spectral/wall-normal space, the former being either the wave length, in the case of spectra, or the separation distance, in the case of the structure function. A first objective has been to examine the properties of turbulence across the spectral range from small-scale motions to the largest resolved motions. To this end, new anisotropy parameters were defined, and maps of these parameters were examined, alongside pre-multiplied and compensated spectra and the pre-multiplied derivative of the second-order structure function, the latter shown to be closely related to the former. Primary emphasis was put on the meso-layer - essentially, the log-law layer spanning the range $80 < y^+ < 2000$.

A first important result derived from the above is a map in wall-normal-distance/wavelength space in which three major sub-ranges were identified within the meso-layer: (A) a sub-range at low wave length (small-scale eddies) in which turbulence is anisotropic, characterised by a dominance of wall-normal and spanwise energy components over the streamwise component and the spectrum $\Phi_{uu} \propto k_x^{-7/3}$; (B) a central range, which conforms to the conventional view of close to isotropic turbulence in which $\Phi_{uu} \propto k_x^{-5/3}$; and (C) a sub-range at high wave length in which the streamwise energy component dominates and in which the spectrum complies with a variation not far from $\Phi_{uu} \propto k^{-1}$. The first result, (A), is rather counter-intuitive, as the expectation is that turbulence in the smallest range of eddies should be close to isotropic. Importantly, the sub-range (C) is not merely confined to the highest

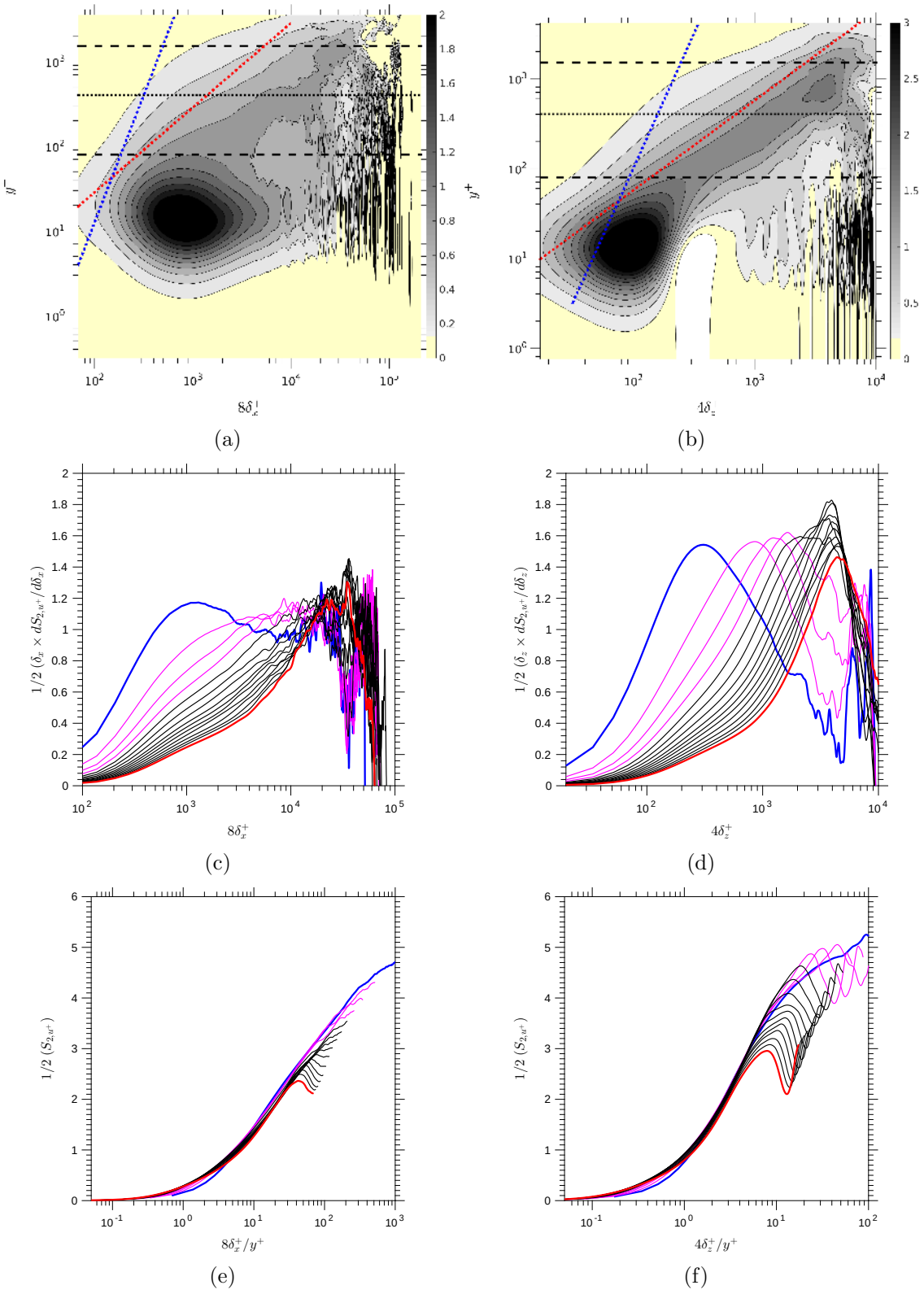

FIG. 16. Statistics for the restricted interval $2800 \leq t^+ \leq 3150$: (a,b) maps of PMDS2 in streamwise and spanwise directions, respectively; (c,d) profiles of PMDS2 as functions of streamwise and spanwise wavelengths, respectively, starting from $y^+ = 100$ (blue line) up to $y^+ = 1200$ (red line) in increments of 100; (e,f) profiles of $S_{2,u}$ as functions of streamwise and spanwise wavelengths, respectively, starting from $y^+ = 100$ (blue line) up to $y^+ = 1200$ (red line) in increments of 100.

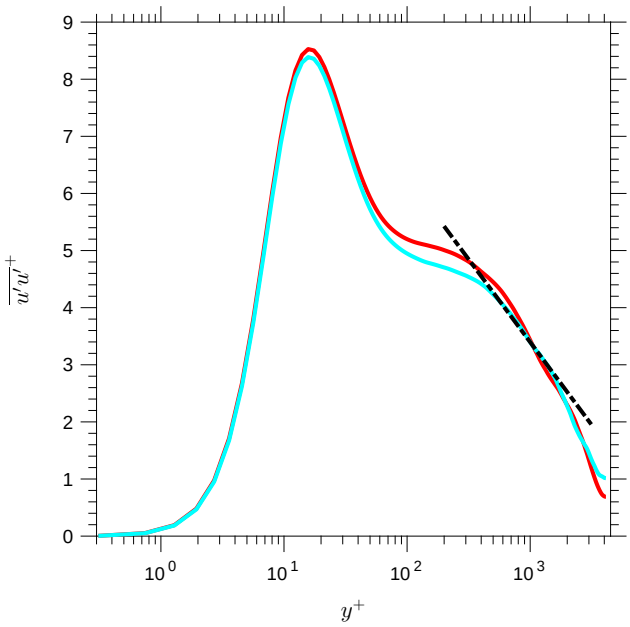

FIG. 17. Wall-normal distribution of the streamwise stress for restricted interval : $2800 \leq t^+ \leq 3150$ (cyan line) and $4200 \leq t^+ \leq 4900$ (red line). The profile derived from the full simulation period is given in figure 1. The dashed line represents the variation $\overline{u'u'}^+ = -1.26 \log y^+ + 12.2$.

wave length, but extends, in lower parts of the log-law meso-layer, well into the range of low wave lengths.

The above investigation, and its results, formed the background against which the second major objective was pursued – namely, to examine whether the attached-eddy hypothesis (AEH) is valid within the meso-layer. To this end, attention focused primarily on the pre-multiplied derivative of the second-order structure function (PMDS2), in preference to the premultiplied spectrum. This preference is based on the observation that the two are closely related, while the latter is a more promising foundation for examining the validity of the AEH – in particular, because the latter brings to light, much more clearly than the former, the tell-tale plateau region with which the AEH is associated. This examination was further aided by the inclusion of one-dimensional PDFs for the streamwise-velocity fluctuations and their streamwise derivative, both displaying significant levels of negative skewness in the meso-layer, and of joined PDFs between the streamwise fluctuations and their streamwise or spanwise derivatives.

A conclusion derived from the PDFs is that the coherent structures in the meso-layer feature a "shape" that is characterized by a broad and short head and a narrow long tail, consistent with existence of a hierarchical structure of attached eddies. Consideration of

the PMDS2 in wall-normal/spanwise-separation space, brought to light a trapezoidal region, contained with the sub-region (C) in the wall-normal/wave-length map, in which the PMDS2 level is close to being constant. Based on conceptual arguments, closely connected to the conventional concept of self-similarity of the scaled energy of attached eddies in a triangular plateau region, the present observations of an approximate plateau in the trapezoidal region led to the conclusion that self-similarity – and hence, the AEH – also applies across the entire meso-layer. An interesting implication of the trapezoidal shape, when assumed transcribable to the spectral map, is that the upper part of the meso-layer is consistent with a logarithmic decay of the streamwise energy, while the lower part of the meso-layer is consistent with a constant level of energy – a behaviour broadly consistent with the directly computed (or measured) y-wise profile of the streamwise energy.

APPENDIX A: ON THE RELATIONSHIP BETWEEN THE SPECTRA AND THE STRUCTURE FUNCTION

First, as noted earlier, $S_{2,u}(\delta)$ may be related to the correlation between the turbulent motions δ apart. If the covariance is defined as $\mathrm{cov}(\delta) = 2\int_0^{+\infty} \Phi_{ii}(\omega)\cos(\omega\delta)d\omega$, where $\omega = 2\pi k_x$ (or $\omega = 2\pi k_z$), the dependence on the correlation function arises from:

$$\begin{aligned} S_{2,u}(\delta) &= \left\langle [u\,(y,x) - u\,(y,x+\delta)]^2 \right\rangle \\ &= \left\langle u\,(y,x)^2 \right\rangle + \left\langle u\,(y,x+\delta)^2 \right\rangle - 2\left\langle u\,(y,x)\,u\,(y,x+\delta)\,\right\rangle \\ &= 2(\mathrm{cov}(0) - \mathrm{cov}(\delta)) \\ &= 2\overline{u'u'}(1 - F_u(\delta)) \end{aligned} \tag{7}$$

$$\frac{dS_{2,u}(\delta)}{d\delta} = -2\overline{u'u'}\frac{dF_u(\delta)}{d\delta} \tag{8}$$

The variation of the correlation function, from its lower limit $F_u(0) = 1$, is monotonic if the signal contained a wide range of eddy sizes (as in turbulent flow) the expectation is that the upper limit is $F_u(L \to \infty) = 0$. For example, $F_u(\delta)$ may be oscillatory if there are quasi-regular "coherent packets" of motion within the range of δ being considered. In the spanwise

direction, the second-order structure function and its derivative, conveyed by figures 7(b) and (d), respectively, brings into focus that the large-scale structures ($\lambda_z \approx 5 \times 10^3$) are strongly coherent in spanwise direction, unlike those in the streamwise direction where no oscillatory behaviour is identifiable in the contour maps shown in figures 7(a) and (c).

Next, the one-dimensional spectrum can be related to the correlation function via the Fourier transform:

$$\Phi_{uu}(k_x) = \frac{2}{\pi} \int_0^{+\infty} F_{u_i}(\delta) \cos(k_x \delta) d\delta \tag{9}$$

Using equations 7 and 9, and the covariance definition given earlier, the following relationship can be derived between the spectra and the structure function:

$$\begin{aligned} S_{2,u_i}(\delta) &= 2 \left[\int_0^{+\infty} \Phi_{uu}(k_x) dk_x - \int_0^{+\infty} \Phi_{uu}(k_x) \cos(k_x \delta) dk_x \right] \\ &= 2 \int_0^{+\infty} (1 - \cos(k_x \delta)) \Phi_{uu}(k_x) dk_x \end{aligned} \tag{10}$$

Consequently, the energy density is related to the derivative of S_{2,u_i} by:

$$\frac{dS_{2,u}(\delta)}{d\delta} = 2 \frac{d}{d\delta} \left[\int_0^{+\infty} (\cos(k_x \delta) \Phi_{uu}(k_x) dk_x \right] \tag{11}$$

The equivalence between δ and λ_x ($= 2\pi/k_x$) is explored here by reference two toy signals of the form:

$$u(x) = \sum_{n=1}^{N} \frac{A}{nk_0} \sin(nk_0 x + \pi) \tag{12}$$

with $N = 1$ or 4. Figure 18(a) shows distributions of $u(x)$, associated spectra, structure function and its derivative for both cases. For $N = 4$, attention is drawn to the fact that the amplitude associated to each mode decreases as the frequency increases, such that $k_i \Phi_i = cst$ ($i = 1, N$), as conveyed by the premultiplied power spectra, which may be interpreted as a discrete version of the AEH.

For $N = 1$, $u(x) = A \cos(k_{x_0} x + \varphi)$, it follows that $\Phi_{uu} = A^2 \delta_d(k_{x_i} - k_{x_0})$, with δ_d being

the Dirac function, and equation 6 then gives:

$$\begin{aligned} \frac{dS_{2,u}(\delta)}{d\delta} &= \frac{d}{d\delta}\left[A^2\cos(k_{x_0}\delta)\right] \\ &= A^2 k_{x_0}\sin(k_{x_0}\delta) \end{aligned} \tag{13}$$

This derivative reaches a maximum for $k_{x_0}\delta = \frac{\pi}{2}$, – i.e. $\delta = \lambda_{x_0}/4$, as is seen in figure 18(d).

When the "coherent" structures arise from several smaller eddies with lower energy, the increase of the $S_{2,u}$ is sharper than in the monochromatic case, with a slope variation associated with the effect of different-sized eddies. The maximum of the derivative of $dS_{2,u_i}/d\delta$ is observed to shift to the left, and this implies a decreasing ratio δ/λ. While the actual value clearly depends on the number of modes (or eddies), and is thus uncertain in real turbulence, it is a fact that the coherent structures are composed of a range of eddies, and this necessarily results in a ratio between δ and λ lower than that for the mono-chromatic case.

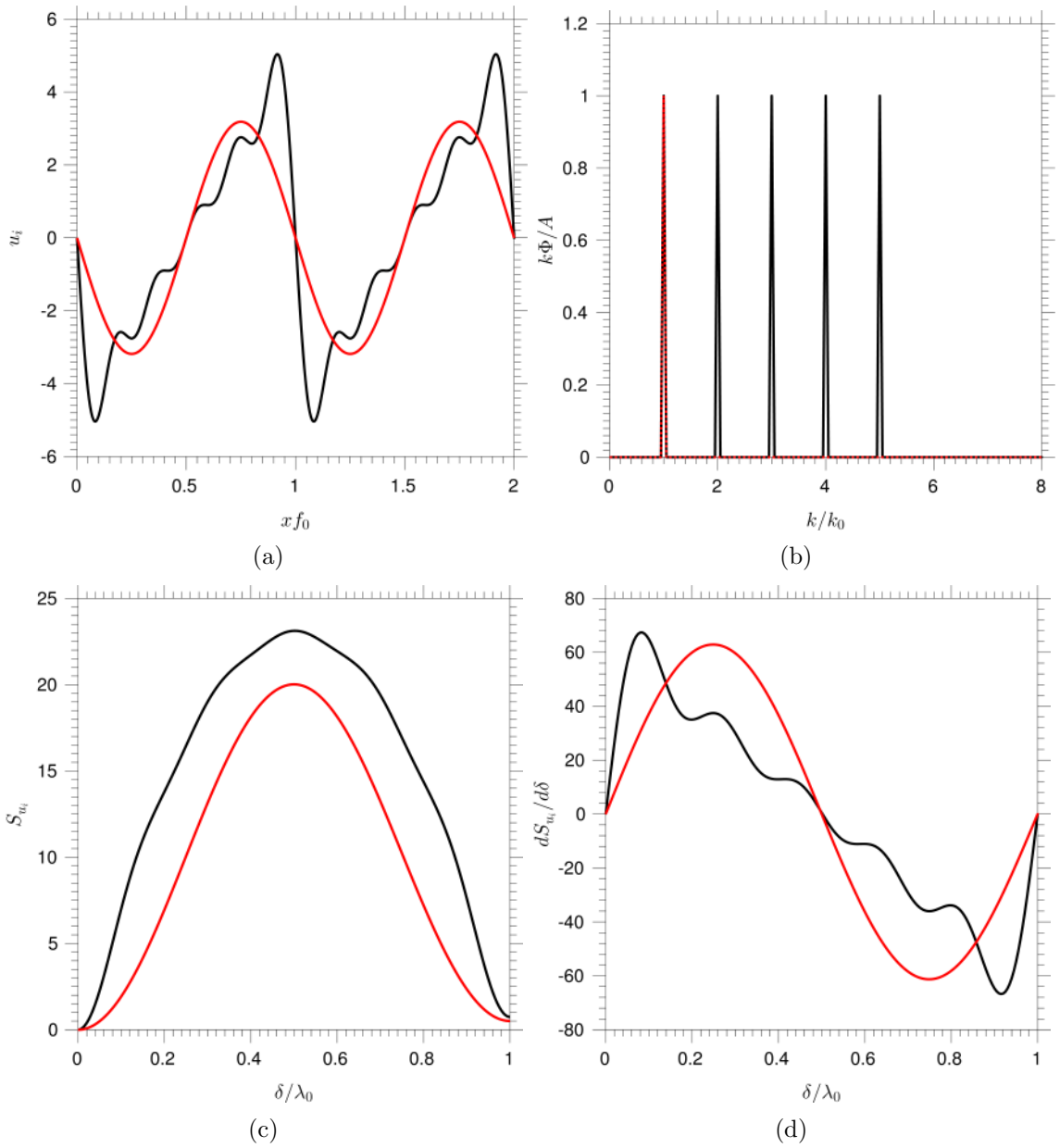

FIG. 18. (a) Toy problems illustrating the relationship between spectra and structure function: (a) signals determined from equations 12 with $N = 1$ and $N = 4$, identified by the red and black lines, respectively; (b) the premultiplied power spectrum for both signals; (c) the second-order structure function and (d) the derivative of the structure function.

ACKNOWLEDGEMENTS

We are grateful to Dr. Lozano-Durán and Prof. Jiménez for making available their DNS database, which formed the basis of the analysis in this paper. We would also like to thank Dr. Lee and Prof. Moser for allowing us to use data derived from their channel-flow DNS

for $Re\tau = 5200$.

REFERENCES

[1]A. A. Townsend, *The structure of turbulent shear flow* (Cambridge university press, 1980).

[2]A. Perry and M. Chong, "On the mechanism of wall turbulence," Journal of Fluid Mechanics **119**, 173217 (1982).

[3]A. Perry, S. Henbest, and M. Chong, "A theoretical and experimental study of wall turbulence," Journal of Fluid Mechanics **165**, 163199 (1986).

[4]A. Perry and I. Marusic, "A wall-wake model for the turbulence structure of boundary layers. Part 1. Extension of the attached eddy hypothesis," Journal of Fluid Mechanics **298**, 361388 (1995).

[5]T. Nickels, I. Marusic, S. Hafez, and M. Chong, "Evidence of the k_1^{-1} law in a high-Reynolds-number turbulent boundary layer," Physical review letters **95**, 074501 (2005).

[6]P. Davidson, T. Nickels, and P.-. Krogstad, "The logarithmic structure function law in wall-layer turbulence," Journal of Fluid Mechanics **550**, 5160 (2006).

[7]P. Davidson, P.-A. Krogstad, T. Nickels, *et al.*, "A refined interpretation of the logarithmic structure function law in wall layer turbulence," Physics of Fluids **18**, 5112 (2006).

[8]C. de Silva, I. Marusic, J. Woodcock, and C. Meneveau, "Scaling of second-and higher-order structure functions in turbulent boundary layers," Journal of Fluid Mechanics **769**, 654–686 (2015).

[9]D. Chung, I. Marusic, J. Monty, M. Vallikivi, and A. Smits, "On the universality of inertial energy in the log layer of turbulent boundary layer and pipe flows," Experiments in Fluids **56**, 110 (2015).

[10]J. Woodcock and I. Marusic, "The statistical behaviour of attached eddies," Physics of Fluids (1994-present) **27**, 015104 (2015).

[11]Y. Hwang, "Statistical structure of self-sustaining attached eddies in turbulent channel flow," Journal of Fluid Mechanics **767**, 254289 (2015).

[12]J. Jiménez and S. Hoyas, "Turbulent fluctuations above the buffer layer of wall-bounded flows," Journal of Fluid Mechanics **611**, 215236 (2008).

[13]I. Marusic, J. P. Monty, M. Hultmark, and A. J. Smits, "On the logarithmic region in wall turbulence," Journal of Fluid Mechanics **716**, R3 (2013).

[14]M. Hultmark, M. Vallikivi, S. Bailey, and A. Smits, "Logarithmic scaling of turbulence in smooth-and rough-wall pipe flow," Journal of Fluid Mechanics **728**, 376395 (2013).

[15]B. Rosenberg, M. Hultmark, M. Vallikivi, S. Bailey, and A. Smits, "Turbulence spectra in smooth-and rough-wall pipe flow at extreme Reynolds numbers," Journal of Fluid Mechanics **731**, 4663 (2013).

[16]A. Lozano-Durán and J. Jiménez, "Effect of the computational domain on direct simulations of turbulent channels up to Reτ= 4200," Physics of Fluids **26**, 011702 (2014).

[17]A. Lozano-Durán and J. Jiménez, "Time-resolved evolution of coherent structures in turbulent channels: characterization of eddies and cascades," Journal of Fluid Mechanics **759**, 432471 (2014).

[18]K. C. Kim and R. J. Adrian, "Very large-scale motion in the outer layer," Phys. Fluids **11**, 417422 (1999).

[19]J. Del Álamo and J. Jiménez, "Spectra of the very large anisotropic scales in turbulent channels," Physics of Fluids **15**, L41 (2003).

[20]N. Hutchins and I. Marusic, "Evidence of very long meandering features in the logarithmic region of turbulent boundary layers," Journal of Fluid Mechanics **579**, 1 (2007).

[21]I. Marusic, R. Mathis, and N. Hutchins, "High Reynolds number effects in wall turbulence," International Journal of Heat and Fluid Flow **31**, 418428 (2010).

[22]R. Mathis, N. Hutchins, and I. Marusic, "Large-scale amplitude modulation of the small-scale structures in turbulent boundary layers," Journal of Fluid Mechanics **628**, 311337 (2009).

[23]J. Vassilicos, J.-P. Laval, J.-M. Foucaut, and M. Stanislas, "The streamwise turbulence intensity in the intermediate layer of turbulent pipe flow," Journal of Fluid Mechanics **774**, 324341 (2015).

[24]N. Hutchins, T. B. Nickels, I. Marusic, and M. Chong, "Hot-wire spatial resolution issues in wall-bounded turbulence," Journal of Fluid Mechanics **635**, 103136 (2009).

[25]M. Hultmark, M. Vallikivi, S. Bailey, and A. Smits, "Turbulent pipe flow at extreme Reynolds numbers," Physical review letters **108**, 094501 (2012).

[26]M. Hultmark, "A theory for the streamwise turbulent fluctuations in high Reynolds number pipe flow," Journal of Fluid Mechanics **707**, 575584 (2012).

[27]A. J. Smits, B. J. McKeon, and I. Marusic, "High-Reynolds number wall turbulence," Annual Review of Fluid Mechanics **43**, 353375 (2011).

[28]M. Lee and R. D. Moser, "Direct numerical simulation of turbulent channel flow up to $Re_\tau \approx 5200$," Journal of Fluid Mechanics **774**, 395415 (2015).

[29]J. Jiménez, "Cascades in wall-bounded turbulence," Annual Review of Fluid Mechanics **44**, 27 (2011).

[30]U. Högström, J. Hunt, and A. Smedman, "Theory and measurements for turbulence spectra and variances in the atmospheric neutral surface layer," Boundary-Layer Meteorology **103**, 101124 (2002).

[31]I. Marusic, "On the role of large-scale structures in wall turbulence," Physics of fluids **13**, 735 (2001).

[32]L. Agostini and M. Leschziner, "On the influence of outer large-scale structures on near-wall turbulence in channel flow," Physics of Fluids **26**, 075107 (2014).

[33]L. Agostini and M. Leschziner, "Predicting the response of small-scale near-wall turbulence to large-scale outer motions," Physics of Fluids **28**, 015107 (2016), 10.1063/1.4939712.

[34]L. Agostini, M. Leschziner, and D. Gaitonde, "Skewness-induced asymmetric modulation of small-scale turbulence by large-scale structures," Physics of Fluids **28**, 015110 (2016).

[35]S. B. Pope, "Turbulent flows," (2001).

[36]M. Vallikivi, B. Ganapathisubramani, and A. Smits, "Spectral scaling in boundary layers and pipes at very high Reynolds numbers," Journal of Fluid Mechanics **771**, 303 (2015).